Calhoun

Institutional Archive of the Naval Postgraduate School

Calhoun: The NPS Institutional Archive

Faculty and Researcher Publications   Faculty and Researcher Publications

1998-11

Modeling Studies of the Leeuwin Current off Western and Southern Australia

Batteen, Mary L.

Modeling Studies of the Leeuwin Current off Western and Southern Australia

MARY L. BATTEEN AND CHRISTOPHER L. BUTLER

Department of Oceanography, Naval Postgraduate School, Monterey, California

ABSTRACT

The Leeuwin Current strengthens considerably from February to May each year, following the slackening of southerly coastal winds; strong eddies develop. A high-resolution, multilevel, primitive equation ocean model is used to examine this eddy development in an idealized way, by considering the development of flow from rest when temperatures are initially given the observed longshore gradients. The system is allowed to geostrophically adjust in the absence of longshore winds and of any surface heat flux. Two types of experiments are conducted. The first type uses the Indian Ocean climatological temperature gradient forcing (case 1 and 2), while the second type repeats the first experiment with the added contribution of the North West Shelf (NWS) temperature profile (cases 3 and 4). To investigate the additional effects of coastline irregularities, cases 1 and 3 use an ideal coastline, while cases 2 and 4 use an irregular (realistic) coastline.

In all cases, maximum surface velocities occur at Cape Leeuwin, where the Leeuwin Current changes direction, and off Southern Australia. Maximum undercurrent velocities occur off Western Australia. In case 1, Cape Leeuwin and the Western Australian coast are the preferred locations for the development of warm, anticyclonic eddies, which are generated due to a mixed instability mechanism. In case 2, the warm, anticyclonic eddies occur in the vicinity of coastal promontories and at Cape Leeuwin. While advection of warm water is present along the entire coast in case 1, the irregular coastline geometry limits the extent of warm water in case 2.

The added contribution from the NWS water in cases 3 and 4 augments the onshore geostrophic inflow to produce a model Leeuwin Current and undercurrent that are more vigorous and unstable than in the previous cases. In case 3, the NWS water adds strong horizontal shear to the coastal equatorial region of the domain and vertical shear to the inshore current. It also advects warmer water along the entire coast. In case 4, the addition of both the NWS water and the irregular coastline results in the establishment of a stronger surface current and undercurrent than in the previous cases; however, the irregular coastline limits the extent of the advection of the NWS warmer water along the Australian coast.

In all cases, warm, anticyclonic eddies develop at the coast. Cold, cyclonic eddies form from the limbs of the established warm, anticyclonic eddies with the result that two counterrotating cells are developed. Once the eddy pairs begin their westward propagation, the Leeuwin Current intensifies as nonlinear effects result in a jet between the eddies and the coast. These effects translate downstream to augment the current velocities at the coast, which, due to a mixed instability mechanism, result in the development of new anticyclonic eddies at the coast.

The results from case 4, which has the most realistic features, highlights the major characteristics of the Leeuwin Current and agrees well with available observations. These results show that the model successfully captures the qualitative nature of the nonlinear, eddying response of the Leeuwin Current.

1. Introduction

The Leeuwin Current is a thermally driven, anomalous, surface eastern boundary current that flows poleward along the Western Australian coast, down to Cape Leeuwin (see Fig. 1 for geographical locations), and swings eastward, extending as far east as the Great Australian Bight (e.g., Cresswell and Golding 1980). There is general agreement (e.g., Godfrey and Ridgway 1985) that the Leeuwin Current is generated by a meridional

pressure gradient, which overwhelms the opposing wind stress. The source for the Leeuwin Current is predominantly geostrophic inflow from the west (e.g., McCreary et. al. 1986; Thompson 1987) and is augmented by a source from the North West Shelf (NWS) (e.g., Gentilli 1972), possibly having its origin in the Pacific Ocean (Hirst and Godfrey 1993). The anomalously warm flow is credited with the appearance of tropical marine species off both the western and southwestern Australian coasts (Pearce and Griffiths 1991). From February to May each year, the Leeuwin Current strengthens considerably and strong eddies develop.

Below the Leeuwin Current, there is an equatorward undercurrent off Western Australia (e.g., Church et al. 1989). Other dynamical features that have been ob-

Corresponding author address: Dr. Mary L. Batteen, Code OC/Bv, Department of Oceanography, Naval Postgraduate School, Monterey, CA 93943-5000.
E-mail: batteen@oc.nps.navy.mil
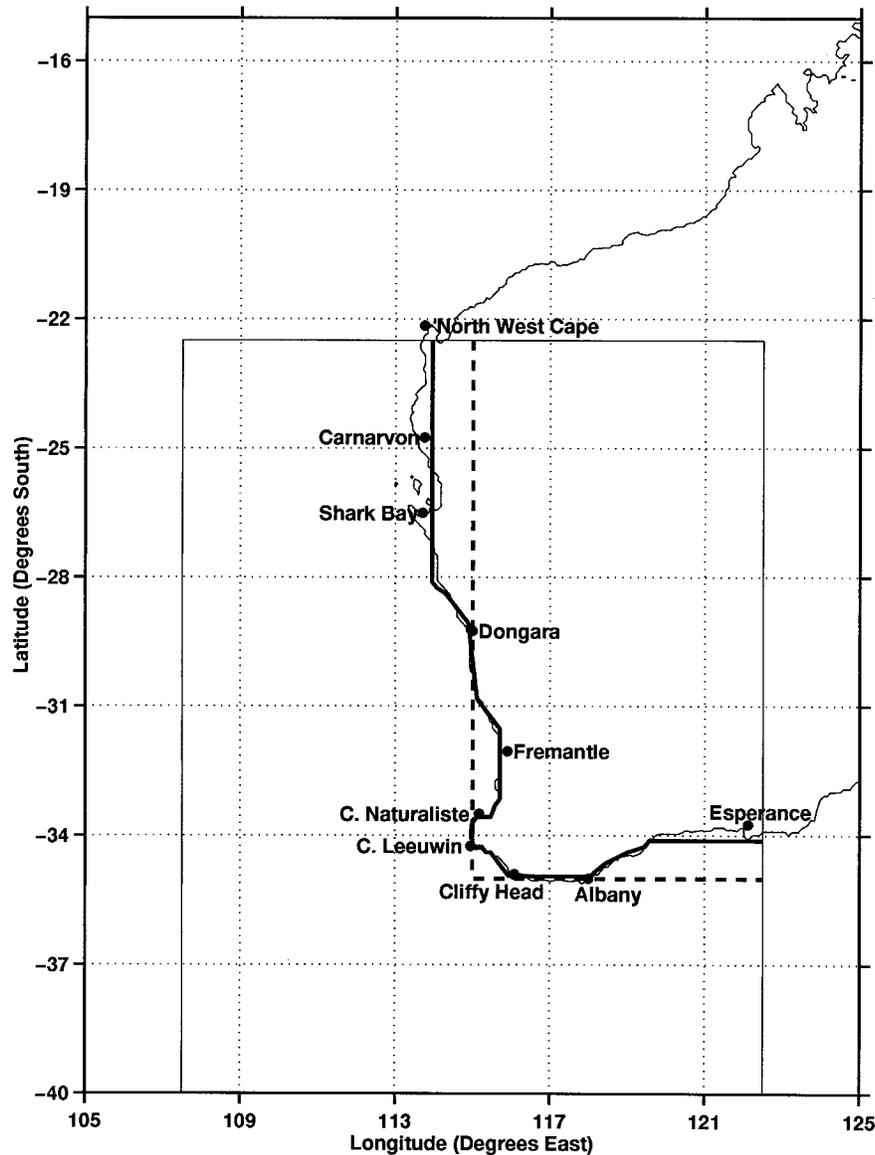
FIG. 1. The model domain (inner box) encompasses the west and south coasts of Australia from 22.5° to 40°S (1792 km), 107.5° to 122.5°E (1408 km). The "ideal coastline" (dashed line) uses a straight line depiction of Western and Southern Australia with Cape Leeuwin represented by a 90-degree corner. The "irregular coastline" (solid line) features the general characteristics and irregularities (e.g., coastal indentation south of Shark Bay, Dongara, Fremantle, Cliffy Head, and Albany) along the west and south coasts of Australia, including a realistic representation of Cape Leeuwin.

served in the Leeuwin Current system (LCS) are off-shoots of the current, meanders, and both anticyclonic and cyclonic eddies (e.g., Legeckis and Cresswell 1981).

Recent satellite images and hydrographic data (Cresswell and Peterson 1993) have shown that the Leeuwin Current undergoes a significant dynamical change as the flow approaches Cape Leeuwin. In particular, the temperature front becomes stronger and more sharply defined. Maximum velocities of ~ 1.8 m s^{-1} near the southwest corner have been observed.

While observations provide insight for the basic na-ture of features in the LCS, process-oriented studies are useful for systematically investigating the characteristics and dynamical forcing mechanisms for the currents and eddies in the LCS. Previous eddy-resolving numerical modeling studies have focused on the dynamics of the Leeuwin Current off Western Australia (e.g., Batteen et al. 1992). To date, no eddy-resolving numerical modeling studies have effectively simulated the Leeuwin Current dynamics and eddy formation mechanisms off the Southern Australian coast. In particular, little is known about the circulation around Cape Leeuwin and

eastward into the Great Australian Bight (Pearce and Cresswell 1985).

This study examines the dynamics of the Leeuwin Current as it translates from north–south to west–east along the Australian coast. With the use of a numerical model, we examine in an idealized way the development of flow from rest when temperatures are initially given the offshore longshore gradients. The system is then allowed to geostrophically adjust in the absence of winds (roughly analogous to the true situation from March on). Other idealizations include the absence of any surface heat flux or mixed layer dynamics, so that changes in our sea surface temperatures are almost entirely due to horizontal advection. With these idealizations, the effects of thermal forcing on the instability mechanisms and current characteristics off Western and Southern Australia will be explored, along with the roles of irregular coastline geometry and the additional contribution of ocean thermal forcing from the NWS water. The organization of the study is as follows: The next section describes the numerical model and the experimental design; section 3 discusses model results, their significance, and a qualitative comparison of model results with observations; and section 4 contains a summary.

2. The model

a. Model description

To investigate the role of thermal forcing on the generation of currents, eddies, and filaments in the LCS, the temperature fields, discussed below, were used to specify the thermal forcing for a high-resolution, multilevel, primitive equation (PE) model of a baroclinic ocean on a β plane. The model is based on the hydrostatic, Boussinesq, and rigid-lid approximations. The governing equations are defined in Batteen (1997). For the finite differencing, a space-staggered B-scheme (Arakawa and Lamb 1977) is used in the horizontal. Batteen and Han (1981) have shown that this scheme is appropriate when the grid spacing is approximately on the same order as, or less than, the Rossby radius of deformation, which meets the criteria of this study. The horizontal grid spacing is 14 km in the north–south direction and 11 km in the east–west direction, while the internal Rossby radius of deformation is ~30 km. In the vertical, the 10 layers are separated by constant z levels at depths of 13, 46, 98, 182, 316, 529, 870, 1416, 2283, and 3656 m. This spacing scheme concentrates more on the upper, dynamically active part of the ocean, above the thermocline.

The model domain (Fig. 1) is a rectangular region encompassing the west and south coasts of Australia from ~22.5° to 40°S (1792 km alongshore) and from ~107.5° to 122.5°E (1408 km cross-shore). The coastal boundaries of the model domain are closed and have both the tangential and normal components of velocity

set to zero. Bottom topography has been omitted to focus on the role played by thermal forcing, as well as the effects of an ideal versus an irregular coastline. The constant depth used in the model is 4500 m.

A modified version of the radiation boundary conditions of Camerlengo and O'Brien (1980) is used for the open-ocean domain boundaries to the north, south, east, and west. In particular, whether a boundary grid point is treated as an inflow point or an outflow point for a particular prognostic variable is determined by the sign of a dynamically computed effective group velocity. This group velocity is defined as the ratio of the local time derivative and the local space derivative normal to the boundary. If the boundary grid point is thereby determined to be an inflow point, then the value of the prognostic variable is set to its value at the previous time step. If the boundary point is determined to be an outflow point, its value is set equal to that of the nearest interior point. Some spatial smoothing is also applied within five grid points (~60 km) of the open boundaries.

The model uses biharmonic lateral heat and momentum diffusion (see Table 1) with the same choice of coefficients (i.e., 2.0×10^{17} cm^4 s^{-1}) as in Batteen et al. (1989). Holland (1978) showed that the highly scale-selective biharmonic diffusion acts predominantly on submesoscales, while Holland and Batteen (1986) found that baroclinic mesoscale processes can be damped by Laplacian lateral heat diffusion. As a result, the use of biharmonic lateral diffusion should allow mesoscale eddy generation via barotropic (horizontal shear) and/or baroclinic (vertical shear) instability mechanisms. As in Batteen et al. (1989), weak (0.5 cm^2 s^{-1}) vertical eddy viscosities and conductivities are used. Bottom stress is parameterized by a simplified quadratic drag law (Weatherly 1972), as in Batteen et al. (1989).

The method of solution is straightforward with the rigid-lid and flat-bottom assumptions because the vertically integrated horizontal velocity is subsequently nondivergent. The vertical mean flow can be described by a streamfunction that can be predicted from the vorticity equation, while the vertical shear currents can be predicted after the vertical mean flow is subtracted from the original equations. The other variables—that is, temperature, density, vertical velocity, and pressure—can be explicitly obtained from the thermodynamic energy equation, equation of state, continuity equation, and hydrostatic relation, respectively (for more complete details on the method of solution, see Batteen 1997).

b. Initial conditions and experimental design

Previous experiments by Batteen and Rutherford (1990) investigated the roles of the Indian Ocean thermal gradients and the NWS water in generating the Leeuwin Current and eddies off Western Australia with a model domain that was a closed eastern boundary with open borders to the north, south, and west. The model was initialized with climatological thermal forcing, and
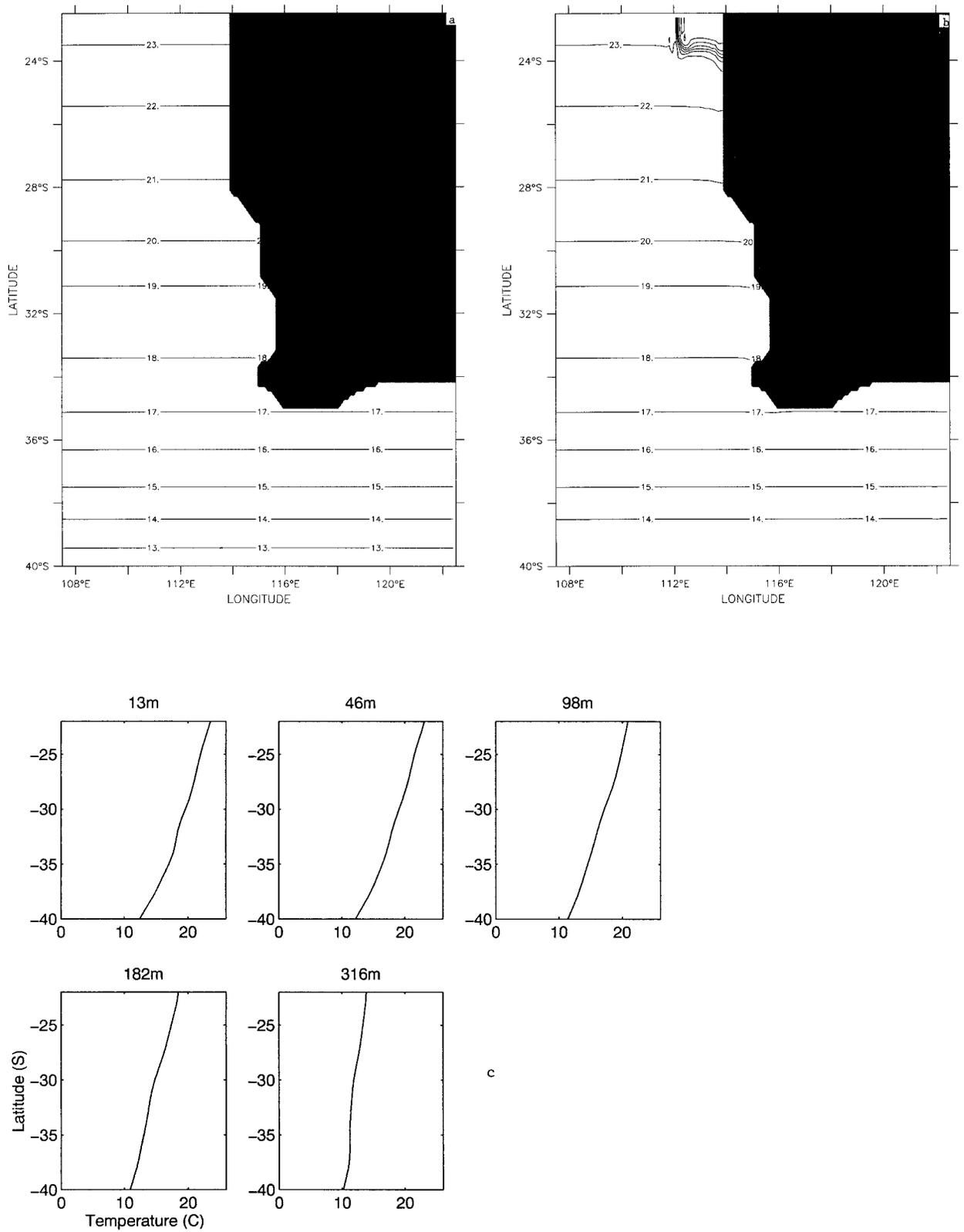
FIG. 2. (a) The initialized fields of surface temperature at depth 13 m for Experiments 1 and 3. (b) The initialized fields of surface temperature with North West Shelf water for experiments 2 and 4. (c) The annual temperature field forcing conditions for the upper five levels at 107.5°E, the western boundary of the model. Since the lower five levels do not have much latitudinal variation, they are assumed to be constant for each level. The contour interval in (a) and (b) is 1 K.

TABLE 1. Values of constants used in the model.

Constant	Value	Definition
T_0	278.2 K	Constant reference temperature
ρ_0	1.0276 gm cm^{-3}	Density of sea water at T_0
α	2.4×10^{-4} K^{-1}	Thermal expansion coefficient
K	10	Number of levels in vertical
Δx	1.1×10^6 cm	Cross-shore grid spacing
Δy	1.4×10^6 cm	Alongshore grid spacing
H	4.5×10^5 cm	Total ocean depth
Δt	800 s	Time step
f_0	0.75×10^4 s^{-1}	Mean Coriolis parameter
g	980 cm s^{-2}	Acceleration of gravity
A_M	2×10^{17} cm^4 s^{-1}	Biharmonic momentum diffusion coefficient
A_H	2×10^{17} cm^4 s^{-1}	Biharmonic heat diffusion coefficient
K_M	0.5 cm^2 s^{-1}	Vertical eddy viscosity
K_H	0.5 cm^2 s^{-1}	Vertical eddy conductivity

TABLE 2. Summary of specific experimental design.

Cases	Ideal coastline utilized?	Irregular coastline utilized?	North West Shelf waters added into model?
1	yes	no	no
2	no	yes	no
3	yes	no	yes
4	no	yes	yes

the ocean was then allowed to geostrophically adjust in the absence of external forcing. The ocean temperature structure used to initialize the experiments in Batteen and Rutherford was considered in two parts with the warmer, less saline NWS water separated from the Indian Ocean waters. Climatological mean temperatures based on Levitus (1982) off Western Australia for both the Indian Ocean and the NWS water were used, and zonal homogeneity was assumed in the Indian Ocean.

In this study, the thermal forcing conditions from Levitus and Boyer (1994) are used to initialize the model and, once a day, to force the model at the western boundary. The annual temperature forcing conditions at the western boundary (107.5°E) for the upper five levels, which are initially assumed to be zonally homogeneous (as seen in Fig. 2a for layer 1), are shown in Fig. 2c. Since the lower five levels do not exhibit much horizontal variation, they are assumed to be constant for each level. The temperature values for levels 6 to 10 are 9.53°, 6.03°, 3.24°, 2.19°, and 1.27°C, respectively. To focus on the role played by thermal forcing, salinity variations are omitted in this study. The constant salinity used is 34.7 psu.

In this study, the model domain has been expanded to include the Southern Australian region, an area rich with observations of currents and eddies, but lacking in eddy-resolving modeling studies of the region. Model developments have included the opening up of the eastern boundary in the vicinity of Esperance in Southern Australia, and the incorporation of idealized and irregular coastlines (see Fig. 1) into the model.

To address the objectives discussed in section 1, four experiments (see Table 2) have been designed. Experiments 1 and 2 study the model response to the climatological thermal forcing (Fig. 2) using the same annual mean temperature gradient for the Indian Ocean, based on Levitus and Boyer (1994). Experiment 1 uses the ideal coastline while experiment 2 uses the irregular coastline. Experiments 3 and 4 study the additional impact of the NWS water (Table 3 and Fig. 2b) on the

Leeuwin Current region using the Indian Ocean climatological mean temperature for mid-March (the timing of which is based on observations of Cresswell and Peterson 1993) to initialize the model. Experiment 3 uses the ideal coastline, while experiment 4 uses the irregular coastline.

3. Results of experiments

a. Experiment 1

1) GENERATION OF CURRENTS AND EDDIES

Due to the initial alongshore temperature field, the resulting pressure gradient establishes an onshore geostrophic inflow from the interior of the ocean. The onshore flow varies between 2 and 10 cm s^{-1}. As the flow approaches the eastern boundary, it turns and forms a narrow poleward boundary current (as seen in Fig. 3a for model day 6), which subsequently enters the Great Australian Bight (with eastward velocities of $\sim$30 cm s^{-1} and accelerating). Additional onshore flow augments the coastal current causing the magnitude of the current to increase in both the poleward and eastward directions. By day 36 (Fig. 3b), maximum velocities of the order of 60 cm s^{-1} are observed near Cape Leeuwin, and maximum velocities of $\sim$70 cm s^{-1} are observed off Southern Australia. After day 36, the onshore geostrophic flow slightly weakens and is maintained at 2–5 cm s^{-1}.

Due to the strong flow of the Leeuwin Current, alongshore temperature gradients are generated at deeper levels, with warm water at the south end of Western Australia and cooler water to the north. These gradients are sufficient to establish an equatorward undercurrent along Western Australia. The strongest equatorward flow is north of Cape Leeuwin ($\sim$20 cm s^{-1}) and is maintained throughout the experiment.

A cross section of meridional velocity (Fig. 4a) shows the typical structure of the poleward Leeuwin Current

TABLE 3. Temperature profile: North West Shelf waters.

Layer	Temperature (°C)
1	29.5
2	28.5
3	26.0
4	20.5
5	15.7
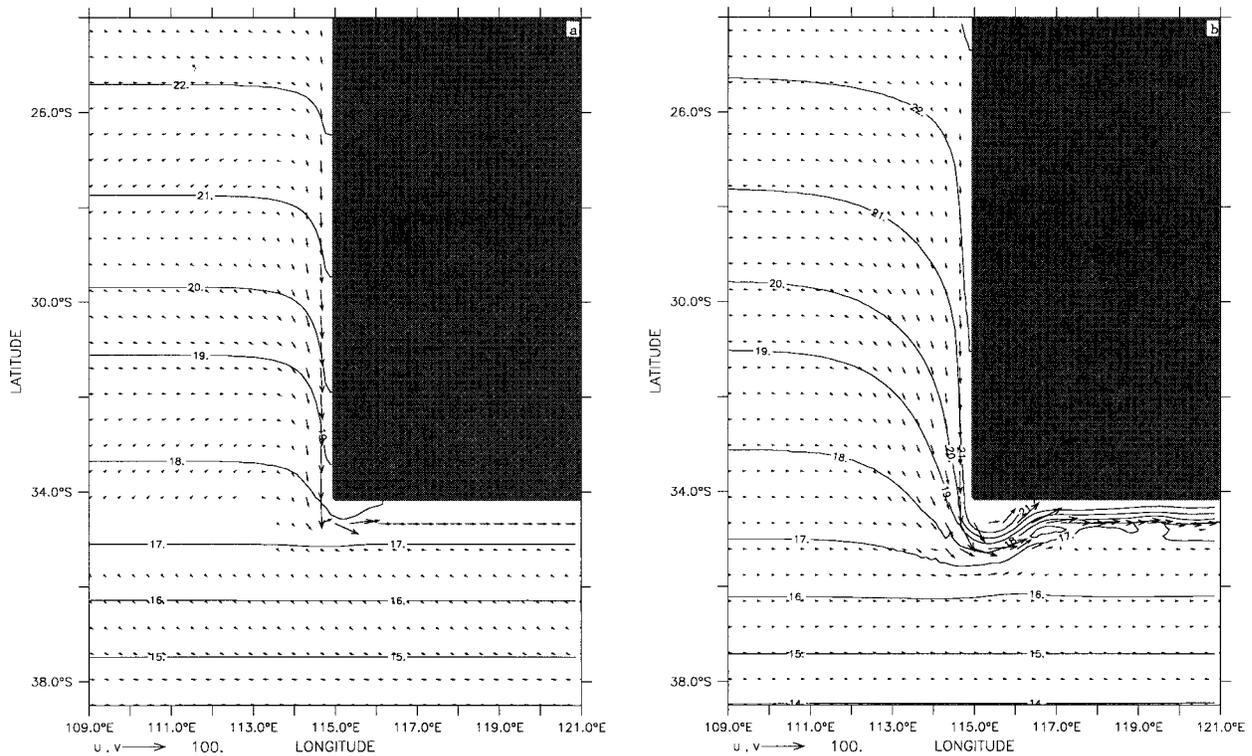
FIG. 3. Experiment 1 surface temperature and velocity vectors at depth 13 m on day (a) 6, (b) 36, (c) 63, (d) 102, (e) 135, (f) 150, and (g) 201. In this and the following figures, to avoid clutter, velocity vectors are plotted at every fourth grid point. The contour interval is 1 K.

and the equatorward undercurrent off Western Australia. The Leeuwin Current jet axis is within ~50 km of the coast and extends from 200 to 400 m depth near the coast. Core velocities range from 40 to 70 cm s^{-1}. A weaker undercurrent with a core velocity of ~20 cm s^{-1} is also seen. The offshore extent of the core of the undercurrent is confined to ~50 km of the coast, while the average core depth is found at ~500 m.

The initial temperature field changes dramatically as the LCS develops. Warm water is rapidly advected poleward and eastward throughout the domain. For example, by day 36 (Fig. 3b), 20°C water has been advected poleward and around Cape Leeuwin and has reached the Great Australian Bight. Additionally at model day 36, 21°C water extends only as far as off the coast of Albany, while 22°C water is only found poleward of ~31°S.

The Indian Ocean climatological thermal gradient is sufficient to establish an unstable flow in the LCS. With the addition of Southern Australia to the model domain, large current offshoots are evident as early as model day 6 (Fig. 3a), as the current shifts from poleward around Cape Leeuwin to eastward toward the Great Australian Bight. These offshoots are likely due to the Coriolis force acting on the flow of the current around the landmass, which would introduce anticyclonic vorticity into the region. An anticyclonic meander in the vicinity of Cape Leeuwin and Albany is established and inten-

sifies with time (e.g., Fig. 3b). Along the south coast of Australia, the current ''jets'' around the Cape Leeuwin meander and continues to accelerate, advecting anticyclonic vorticity downstream and intensifying undulations and offshoots upstream of Esperance (entrance to the Great Australian Bight). The eastward current magnitude is greater toward the coast and decreases offshore. Nearshore the current velocity varies as nonlinear feedback causes surges from ~70 cm s^{-1} at day 36 (Fig. 3b) to ~90 cm s^{-1} by day 63 (Fig. 3c).

The mesoscale features in the current intensify and grow, such that by day 63 (Fig. 3c), the Cape Leeuwin meander develops into an anticyclonic eddy. Undulations in the poleward current intensify as far up the coast as Dongara. By day 102 (Fig. 3d), an anticyclonic eddy forms in the vicinity of Fremantle. Meanders upstream of Esperance simultaneously intensify. By day 135 (Fig. 3e), the Fremantle anticyclonic eddy begins a westward propagation. The poleward Leeuwin Current intensifies as nonlinear effects result in a ''jet'' between the eddy and the coast. These effects translate downstream to augment the current off Western and Southern Australia.

Between days 135 and 150 (Fig. 3f), another anticyclonic eddy has formed off the coast of Fremantle. Between the coastal and offshore anticyclonic eddies, a cyclonic eddy has also developed, which propagates westward, traveling with the offshore anticyclonic eddy as an eddy pair. Between Fremantle and Cape Leeuwin
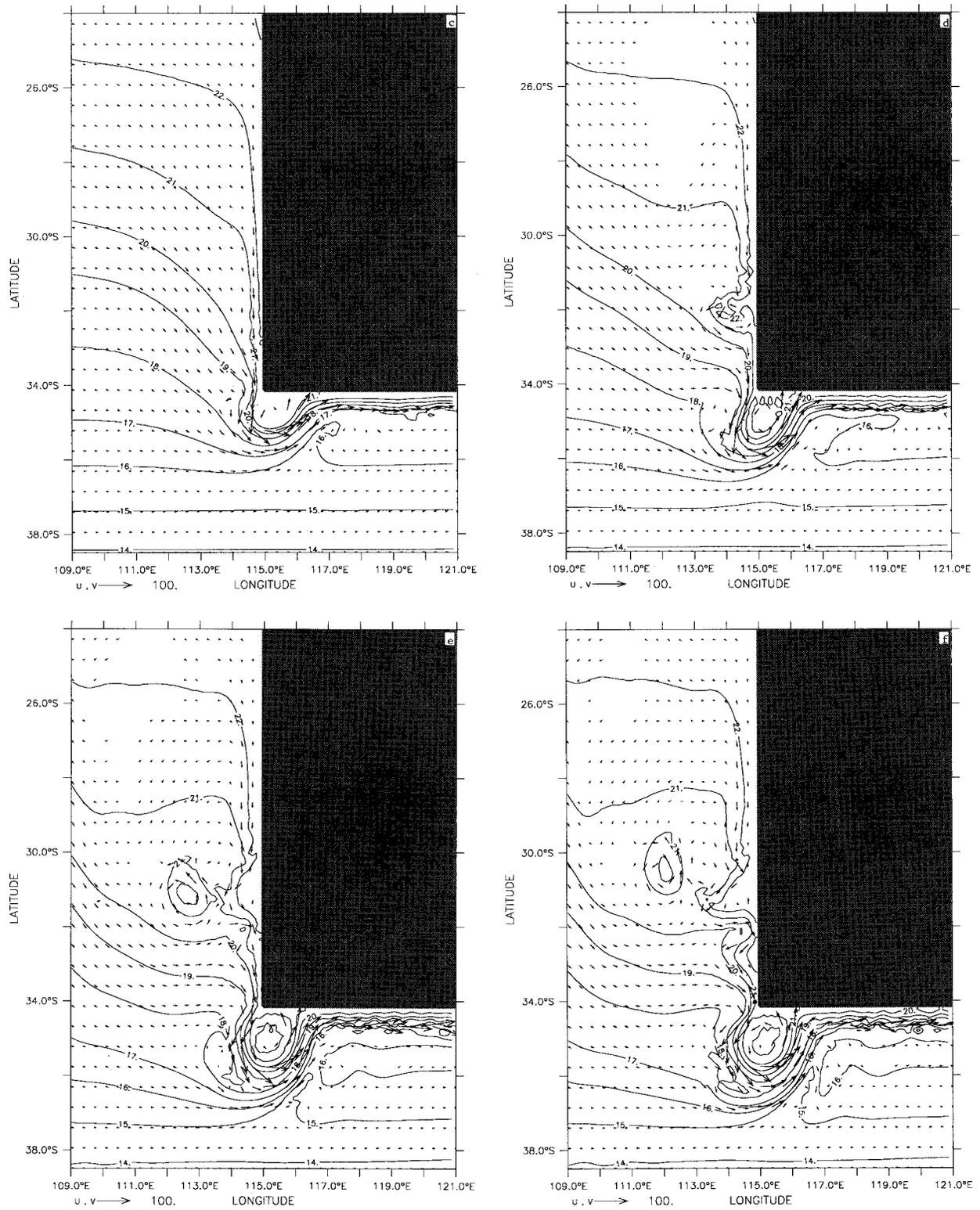
FIG. 3. (*Continued*)
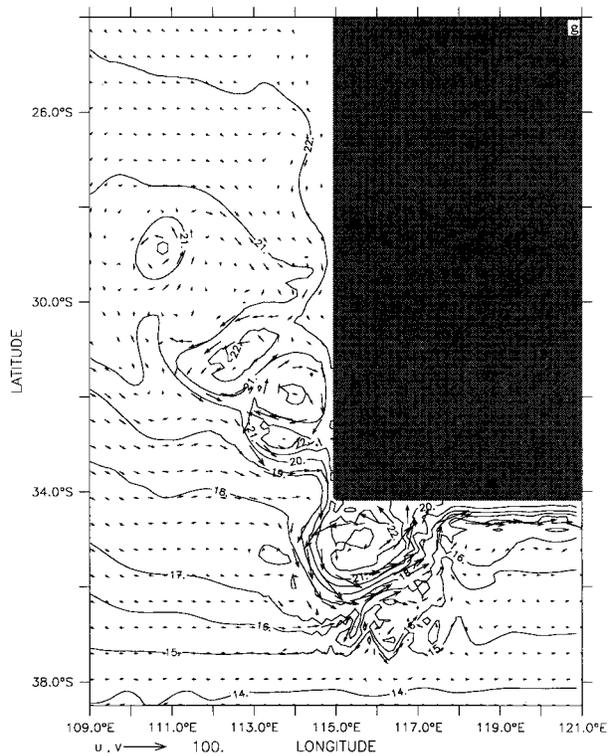
FIG. 3. (*Continued*)

an anticyclonic meander develops. Farther south, a weak cyclonic eddy forms by day 201 (Fig. 3g) from offshoots on the offshore side of the anticyclonic limb of the Cape Leeuwin eddy. It subsequently propagates downstream on the offshore side of the Leeuwin Current off Southern Australia.

The formation of eddies contributes to a significant amount of advection of warm water offshore by the anticyclonic eddies (e.g., Fig. 3f). The warm core eddy in the vicinity of Fremantle propagates westward and brings 22°C water into the interior ocean. The Cape Leeuwin warm core eddy also embodies 22°C water that spans the offshore waters of the cape, while the Cape Leeuwin cold core meander embodies 16°C water and, in time, establishes a sharp temperature front in the periphery of the eddy pair as the meander continues to intensify. The Leeuwin Current is augmented by off-shoots of warmer water released downstream into coast-al regions previously blocked by warm core meanders and eddies. These offshoots act to enhance further me-soscale development, as pools of warm water entrain into the core of downstream meanders and eddies.

2) ANALYSIS OF EDDY GENERATION MECHANISMS

The dynamical reasons for the generation and stability of eddies in the Leeuwin Current system are examined using the energy techniques used and described by Bat-teen et al. (1992). From the energy transfer analysis, the location and magnitude of baroclinic and barotropic transfers can be found and examined to argue for the type of instability mechanism (e.g., barotropic, baro-clinic, or mixed), which leads to the initial eddy gen-eration.

Analysis of Fig. 4a shows that there is considerable horizontal and vertical shear in the upper-layer currents off Western Australia. Barotropic instability can result from horizontal shear in the currents, while baroclinic instability can result from vertical shear in the currents. As a result, both types of instability (mixed) can be present simultaneously. Energy transfer calculations, which consist of barotropic (mean kinetic energy to eddy kinetic energy) and baroclinic (mean potential en-ergy to eddy potential energy to eddy kinetic energy) components were performed for the time periods when the meanders and eddies developed.

Results for the instability analysis (not shown) show that both barotropic and baroclinic (i.e., mixed) insta-bility mechanisms are present in the coastal region off Western Australia, while barotropic instability domi-nates in the coastal regions off Cape Leeuwin and Southern Australia. In particular, off Western Australia mixed instabilites are responsible for the eddy devel-opment that occurred off Fremantle by day 102 and between days 135 and 150. Off Cape Leeuwin, baro-tropic instability is responsible for the eddy develop-ment between days 36 and 63. Mixed instability trans-fers, with barotropic instability dominant over baroclinic instabilty, are responsible for the cyclonic meanders that developed by day 201 on the offshore side of the Cape Leeuwin eddy.

Horizontal maps of the upper-layer mean kinetic en-ergy (MKE) and eddy kinetic energy (EKE), averaged over the duration of the time period when the Leeuwin Current is strongest (~180 days), are shown in Figs. 5a and 5b. Maps of MKE and EKE are suggestive of where the mean and eddy energy sources are to be found (Hol-land et al. 1983). High values of MKE and EKE are found off Southern Australia, while high values of EKE are also found off Western Australia south of 30°S. A comparison of Figs. 5a and 5b show that, overall, the MKE is larger than the EKE. This is consistent with the model simulations that showed that the eddies are gen-erated from instabilities of the mean currents via bar-otropic and/or baroclinic instability processes.

b. *Experiment 2*

1) GENERATION OF CURRENTS AND EDDIES

In experiment 2, the initial current characteristics are similar to the initial characteristics of experiment 1. In particular, both a poleward and equatorward surface cur-rent develop (e.g., Figs. 6a and 6b), and an equatorward undercurrent is established off Western Australia (e.g., Fig. 4b).

The initial temperature field changes less dramatically
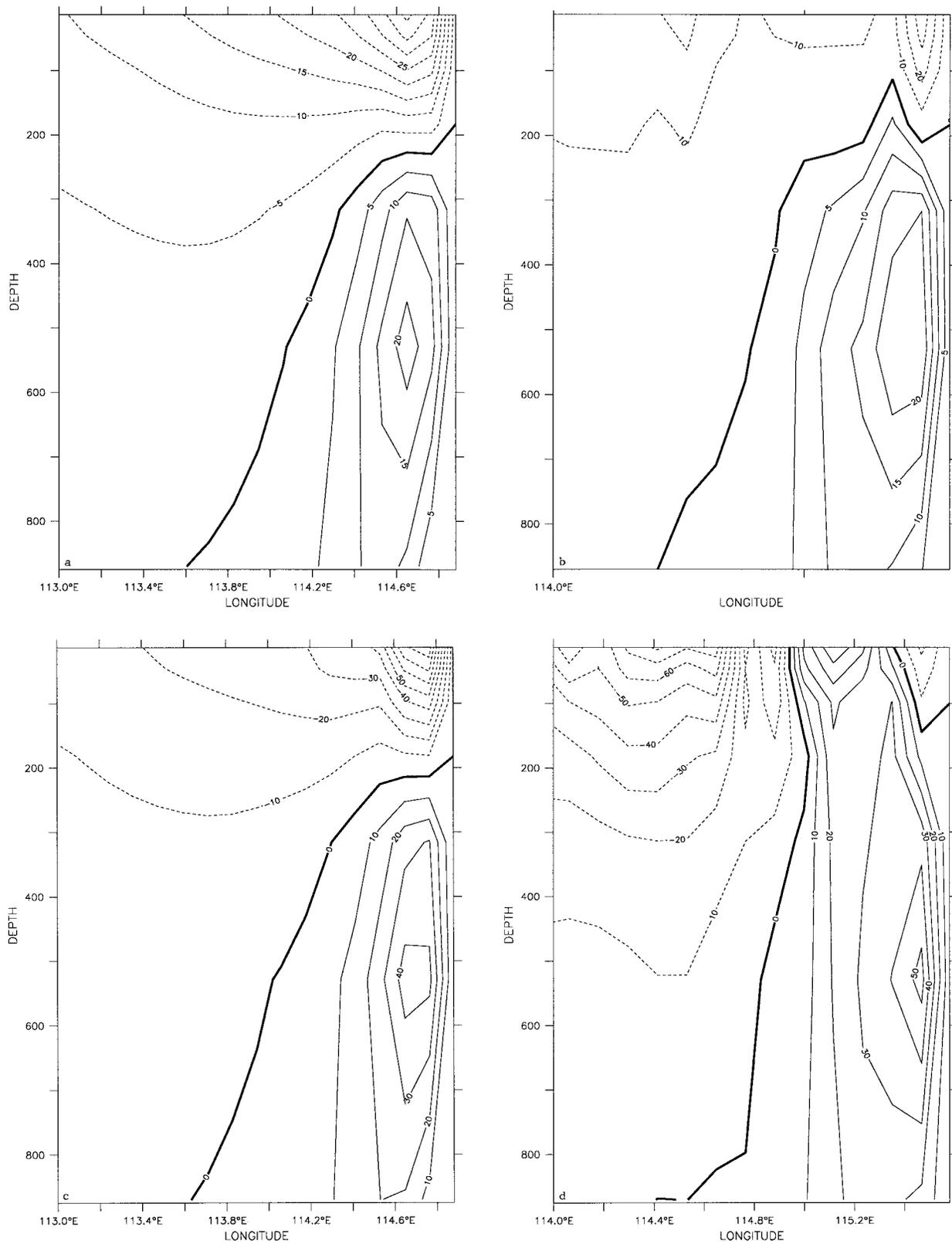
FIG. 4. Cross-shore sections of the meridional component of the velocity field at 32.5°S at day 36 for (a) experiment 1, (b) experiment 2, (c) experiment 3, and (d) experiment 4. Solid lines indicate equatorward flow, while dashed lines indicate poleward flow. The contour interval for poleward flow is 5 cm s⁻¹ in (a) and 10 cm s⁻¹ in (b)–(d). The contour interval for equatorward flow is 5 cm s⁻¹ in (a) and (b) and 10 cm s⁻¹ in (c) and (d).
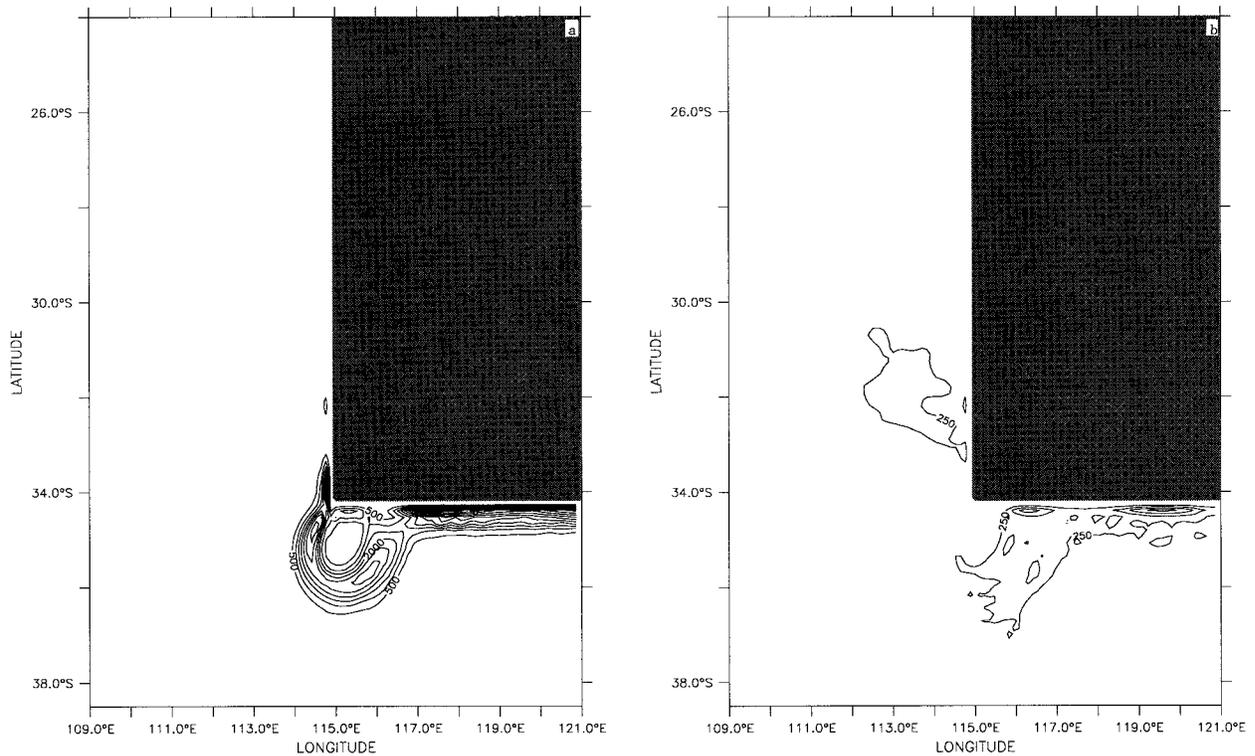
FIG. 5. Mean (a) and eddy (b) kinetic energy for experiment 1 at 13-m depth, averaged over 180 days (from days 90 to 270), when the Leeuwin Current is strongest. The contour interval is 500 cm² s⁻² in (a) and 250 cm² s⁻² in (b).

than in experiment 1, as the LCS develops along the irregular coastline. For example, by day 36 (Fig. 6b), 19°C water has been advected poleward and around Cape Leeuwin and has reached the Great Australian Bight; however, 20°C water only extends as far as off the coast of Albany, 21°C water only as far as the coast off Fremantle, and 22°C water only as far as Dongara.

The addition of an irregular coastline results in significant instability at preferred locations from the onset of the model run. Large current offshoots, evident by model day 6 (Fig. 6a), occur along the west coast irregular coastline and around Cape Leeuwin where the current changes direction. Anticyclonic meanders (one just south of Shark Bay, one between Dongara and Fremantle and one in the vicinity of Cape Leeuwin and Cliffy Head) are established and instabilities subsequently intensify. The growth of these meanders effects the current characteristics both upstream and downstream. By day 36 (Fig. 6b) the current along the west coast of Australia has large undulations near the Shark Bay and Fremantle meanders.

Along the south coast of Australia, the current jets around the Cape Leeuwin meander and continues to accelerate, advecting anticyclonic vorticity downstream and intensifying undulations and offshoots upstream of Esperance. Nearshore the current velocity varies (due to nonlinear feedback causing surges) from ~75 cm s⁻¹ at day 36 (Fig. 6b) to ~95 cm s⁻¹ by day 45 (Fig. 6c).

The eastward current magnitude is greater toward the coast and decreases offshore.

The mesoscale features in the current intensify and grow. By day 45 (Fig. 6c), the Shark Bay, Fremantle, and Cape Leeuwin meanders develop into anticyclonic eddies. The poleward current jets around these meanders. Offshoots and meanders encompass the entire coast of Southern Australia well into the Great Australian Bight. By day 72 (Fig. 6d), an anticyclonic eddy forms in the LCS Southern Australian branch near Albany. Additionally, within this time frame a cyclonic eddy develops west of Albany, a cyclonic meander southwest of Esperance intensifies, and the Shark Bay and Fremantle eddies begin their westward propagation. By day 144 (Fig. 6e), the Shark Bay, Fremantle, and Cape Leeuwin anticyclonic eddies have propagated westward well into the interior ocean. The westward propagation speeds are 5–10 km day⁻¹, consistent with Rossby wave propagation speeds.

Eddy pairs are clearly visible throughout the coastal region. Cold, cyclonic eddies form from the anticyclonic limb of the established warm core eddies with the result that two counterrotating cells are developed. As the eddies begin their westward propagation, the poleward Leeuwin Current intensifies as nonlinear effects result in a jet between the eddies and the coast. These effects translate downstream to augment the current velocities off Southern Australia. As instabilities along the coast

continue, new anticyclonic eddies form off Shark Bay and Dongara. In time, the Leeuwin Current anticyclonic eddy detaches and propagates northwestward. While there is no Cape Leeuwin eddy present, the cyclonic eddies off Southern Australia intensify in time and begin a westward propagation. By day 333 (Fig. 6f), a new anticyclonic eddy develops between Cliffy Head and Albany, and the cyclonic eddies off Southern Australia propagate to the west on the offshore side of the anticyclonic eddy.

As in experiment 1, the formation of eddies contributes to a significant amount of advection of warm water offshore by the anticyclonic eddies (e.g., Fig. 6e). For example, the warm core eddy in the vicinity of Shark Bay propagates northwestward and brings 22.5°C water into the interior ocean. The warm core eddy in the vicinity of Fremantle propagates westward and brings 21°C water into the interior ocean. The Cape Leeuwin warm core eddy embodies 19°–20°C water, which spans the offshore waters of the cape, while the cold core eddy embodies 16°C water and establishes a sharp temperature front in the peripheral of the eddy pair as the meander continues to intensify. The current is augmented by upstream offshoots of warmer water released downstream into coastal regions previously blocked by warm core meanders and eddies. These offshoots act to enhance mesoscale development, as pools of warm water entrain into the core of downstream meanders and eddies.

2) ANALYSIS OF EDDY GENERATION MECHANISMS

Analysis of horizontal plots of energy transfers are used to find the location and magnitude of both barotropic and baroclinic transfers. Examination of the magnitudes of both barotropic and baroclinic instability mechanisms (not shown) for the 39–63 day period, corresponding to the period of eddy generation for the Shark Bay, Fremantle, and Cape Leeuwin eddies, shows that mixed instability is responsible for the generation of the eddies, with barotropic instability dominating over baroclinic instability. This is also the case for eddy development at days 72 and 144.

Horizontal maps of the upper-layer MKE and EKE, averaged over the time period when the Leeuwin Current is strongest (~180 days), are shown in Figs. 7a and 7b. High values of MKE (Fig. 7a) are found off Cape Leeuwin and Southern Australia. High values of EKE (Fig. 7b) are found south of 30°S all along the coastal and offshore regions of Western and Southern Australia. The highest values of MKE and EKE are found in the coastal regions off Southern Australia.

c. Experiment 3

1) GENERATION OF CURRENTS AND EDDIES

With the addition of the NWS water to the climatological thermal gradient of the Indian Ocean, a more energetic and dynamic current than that in the previous experiments is established. From the onset of the model run, the NWS water adds strong horizontal shear to the coastal equatorial region of the domain, and vertical shear to the inshore current. Away from the source region, the influence of the NWS water diminishes poleward, but is still strong enough to augment the onshore geostrophic inflow with the result that a stronger current is established throughout the coastal regions of Western and Southern Australia. The initial onshore geostrophic inflow from the interior of the ocean is of the same magnitude (i.e., ~2–10 cm s^{-1}) as in the previous experiments; however, the narrow poleward boundary current has magnitudes on the order of 150 cm s^{-1} off Shark Bay and 110 cm s^{-1} just south of Dongara by day 6 (Fig. 8a). The current entering the Great Australian Bight is larger than that of the previous experiments with a magnitude of 40 cm s^{-1} and accelerating, as shown in Fig. 8a. Continual onshore geostrophic inflow and nonlinear feedback mechanisms augment the poleward and eastward current. By day 18 (not shown), the poleward current has reached a maximum of 180 cm s^{-1} at Cape Leeuwin. The eastward current continues to accelerate from ~40 cm s^{-1} at day 6 (Fig. 8a) to ~160 cm s^{-1} at day 36 (Fig. 8b).

The addition of the NWS water also results in the establishment of a stronger undercurrent than in the previous experiments. The strongest equatorward flow (45 cm s^{-1}) is north of Cape Leeuwin at day 12 (not shown). It subsequently decreases to ~40 cm s^{-1} by day 36 (Fig. 4c) and maintains this speed throughout the experiment. The average core depth of the undercurrent is at 500 m.

The initial temperature field changes dramatically due to the addition of the NWS water. The advection of the NWS water results in a narrow core of warmer water along the entire coastal boundary. By day 36 (Fig. 8b), 23°C water has been advected poleward and around Cape Leeuwin and has reached the Great Australian Bight, while 24°–25°C water extends around Cape Leeuwin to just west of Albany. A strong temperature front is also established along the Southern Australian coast.

The addition of the NWS water adds significant instability to the source region and throughout the coastal regions of Western and Southern Australia. As a result of this more vigorous and unstable current, an earlier eddy generation period than in the previous experiments is observed. The stronger surface current, along with the NWS water temperature gradient produces a large horizontal shear zone in the coastal equatorial region. Coupled with a stronger undercurrent, greater baroclinic instability contributes to a larger vertical shear zone throughout the entire coastal region. As early as day 6 (Fig. 8a), an anticyclonic meander is formed near the source region, and large offshoots are observed at Cape Leeuwin. Instabilities intensify such that by day 36 (Fig. 8b), a large undulation occurs in the current along both the western and southern coastal branches resulting in anticyclonic meanders, one just south of Shark Bay, and
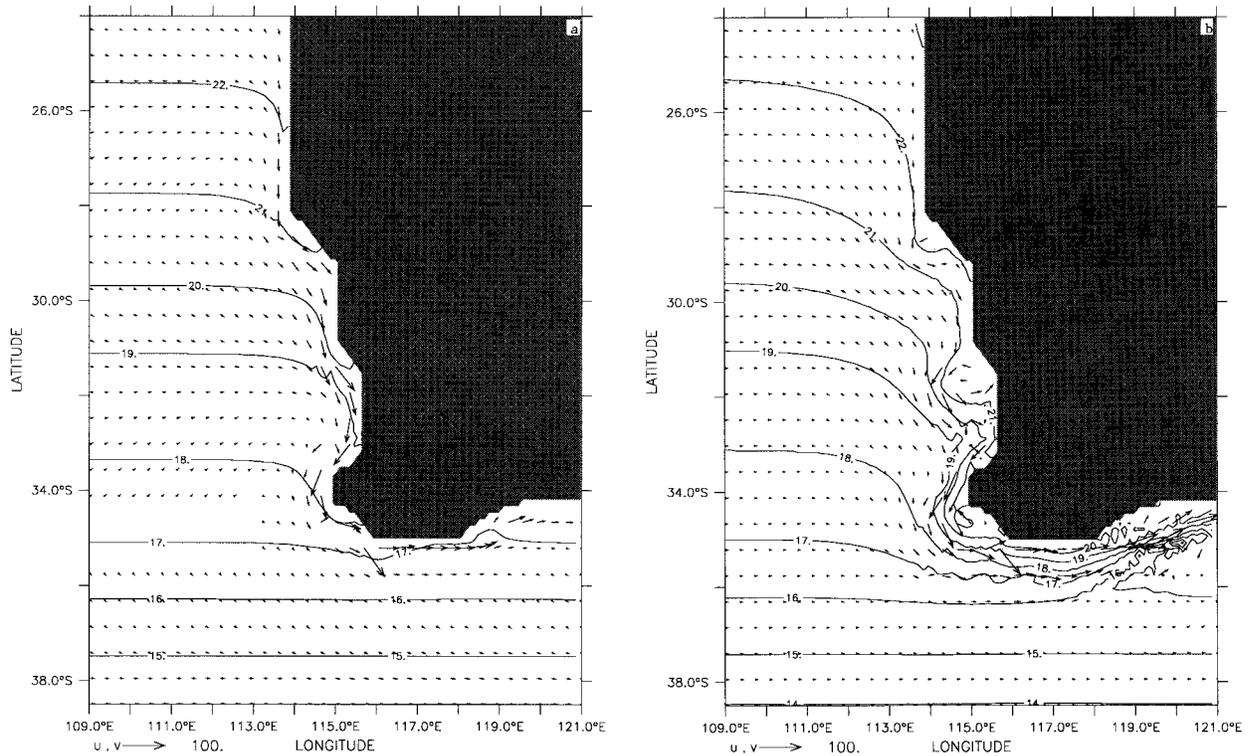
FIG. 6. Experiment 2 surface temperature and velocity vectors at depth 13 m on day (a) 6, (b) 36, (c) 45, (d) 72, (e) 144, and (f) 333. The contour interval is 1 K.

one at Cape Leeuwin. Current offshoots occur in the vicinity of Fremantle and east of Albany. Nonlinear feedback continues to increase the current surges along both the western and southern coasts of Australia.

The mesoscale features rapidly form eddies. For example, the current characteristics at day 45 (Fig. 8c) show anticyclonic eddies near the NWS water source region, Shark Bay, Fremantle, and Cape Leeuwin. Offshoots and meanders encompass the entire coast of Australia. By day 129 (Fig. 8d), the NWS, Shark Bay, and Fremantle eddies have begun to propagate westward, and a cyclonic eddy has formed from the anticyclonic limb of the Cape Leeuwin eddy. An eddy pair is also visible between Dongara and Fremantle.

Since the NWS water addition advects warmer water throughout the entire Australian coast, it also results in the advection of warmer waters offshore by the anticyclonic eddies. Overall, the eddies developed in experiment 3 are 2°–4°C warmer (e.g., see Fig. 8d) than the initial eddies formed in the previous experiments.

2) ANALYSIS OF EDDY GENERATION MECHANISMS

The energy transfers for days 36 to 63 (not shown), which correspond to the same eddy generation period as experiment 1, show mixed instabilities present with the barotropic instability mechanism dominant off Cape

Leeuwin. This is also the case for eddy development for days 114 to 141; however, analysis of the energy transfers off Western Australia reveals that baroclinic instability dominates over barotropic instability. This could possibly be caused by the interaction of northern eddy pairs propagating westward and the onshore geostrophic eastward flow with the result that transitory vertical shear regions are generated.

Figures 9a and 9b show horizontal maps of the upper-layer MKE and EKE, averaged over the duration of the time period when the Leeuwin Current is strongest (~180 days). As in experiment 1, the highest values of MKE (Fig. 9a) and EKE (Fig. 9b) are found off Cape Leeuwin and off Southern Australia. High values of EKE are also found all along the Western Australian coastal and offshore regions, in contrast to experiment 1, which showed high values of EKE confined to ~30° and 34°S off Western Australia. The high values all along the Western Australian coast are likely due to the NWS water addition, which adds significant instability to the source region and throughout the coastal region of Western Australia.

d. Experiment 4

1) GENERATION OF CURRENTS AND EDDIES

As expected, the addition of both the NWS water and the realistic irregular coastline introduces even greater
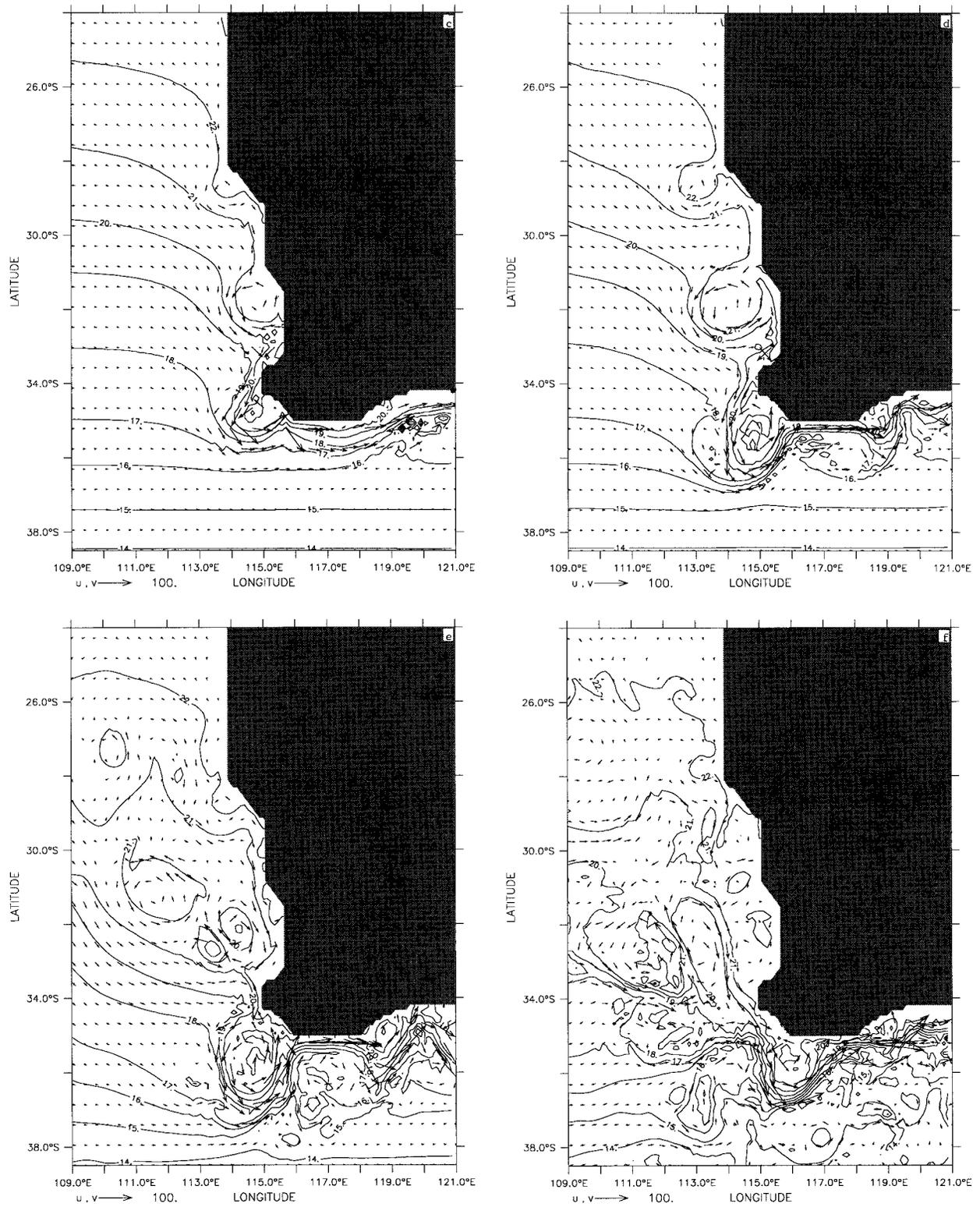
FIG. 6. (*Continued*)
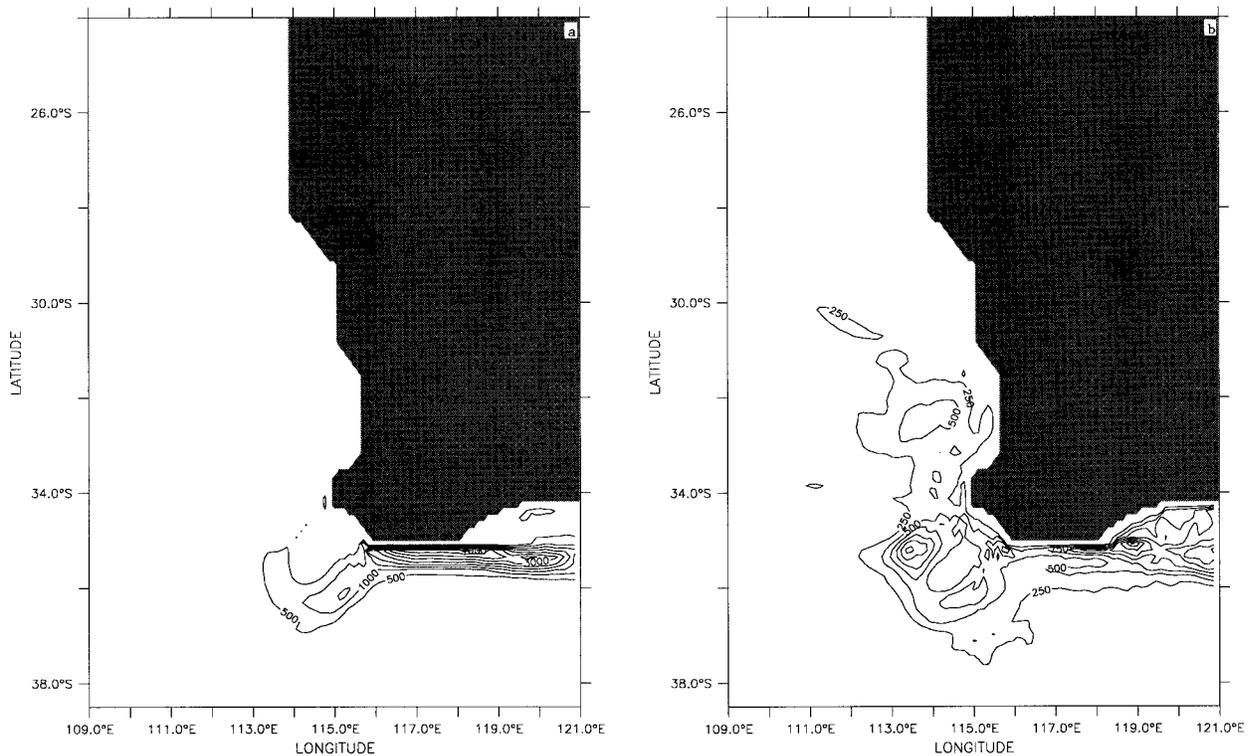
FIG. 7. Same as Fig. 5 except for experiment 2.

instabilities into the model LCS than in the previous experiments. Current velocities of the poleward boundary current are generally higher than those established in experiment 3. A new regional maximum of 180 cm s^{-1} is observed off of Shark Bay by day 9 (Fig. 10a). Also by day 9, the current velocity at Cape Leeuwin is 135 cms^{-1}, and the eastward current is 120 cm s^{-1} and accelerating. By day 12 (not shown), the Cape Leeuwin poleward velocity peaks at 170 cm s^{-1} and the eastward current peaks at 160 cm s^{-1}. By day 24 (Fig. 10b), the current velocities have decreased to ~100 cm s^{-1}, which are maintained throughout the experiment.

The addition of both the NWS water and the irregular coastline results in the establishment of a stronger undercurrent. The strongest equatorward flow (60 cm s^{-1}) is north of Cape Leeuwin at day 24. It subsequently decreases to ~50 cm s^{-1} (e.g., Fig. 4d) and maintains this speed throughout the experiment. As in the previous experiment, the average core depth of the undercurrent is at ~500 m.

As in experiment 2, the irregular coastline limits the extent of the advection of the NWS warmer waters along the Australian coast. For example, by day 24 (Fig. 10b), only 19°C water has been advected into the Great Australian Bight; the 20°C water extends between the coast of Albany and Esperance; the 21°C water extends around Cape Leeuwin; and the 22°–24°C waters are found only as far south as Fremantle.

As in experiment 3, as early as day 9 (Fig. 10a), an anticyclonic meander develops near the coast of the NWS water source region. As in experiment 2, current shifts along the irregular coastline produce undulations and large offshoots. For example, by day 9 (Fig. 10a), large offshoots are observed near Shark Bay, Fremantle, around Cape Leeuwin, and as far east as Albany. By day 24 (Fig. 10b), these offshoots intensify to form anticyclonic meanders. By day 36 (Fig. 10c), anticyclonic eddies have formed near the coast of the NWS water source, at Shark Bay, Fremantle, and in the vicinity of Cape Leeuwin and Cliffy Head. By day 90 (Fig. 10d), the west coast eddies have begun their westward propagation, and cyclonic eddies have formed from the limbs of the anticyclonic eddies. Regional instabilities continue to intensify such that by day 120 (Fig. 10e), an anticyclonic eddy has formed off the coast of Dongara, and eddy pairs are established all along the western and southern coasts of Australia.

2) ANALYSIS OF EDDY GENERATION MECHANISMS

Analysis of horizontal plots of the energy transfer for days 24–45 (not shown), covering the time period for the formation of the Shark Bay, Fremantle, Cape Leeuwin, and Cliffy Head eddies, shows that mixed instabilities are present with barotropic instability mecha-
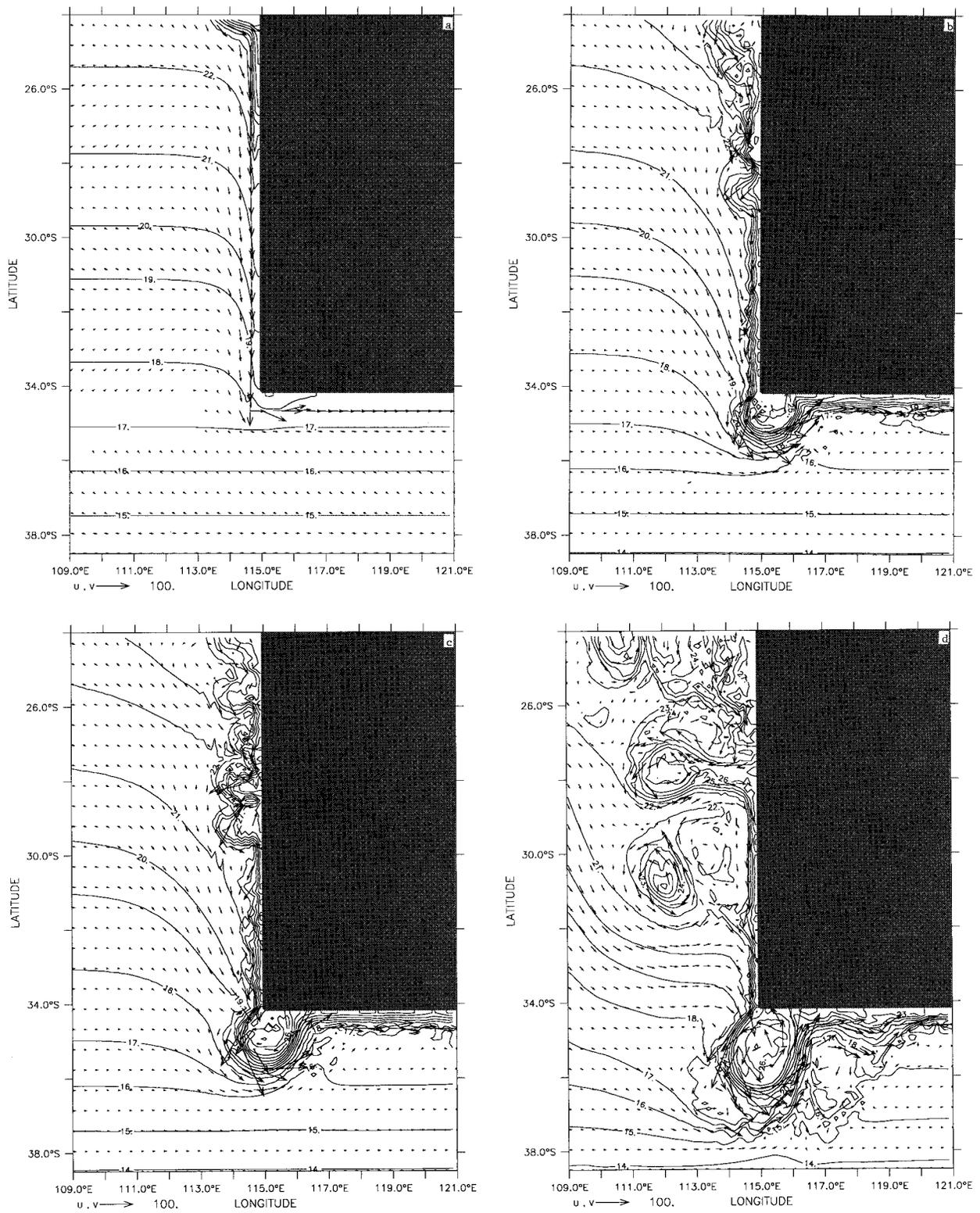
FIG. 8. Experiment 3 surface temperature and velocity vectors on day (a) 6, (b) 36, (c) 45, and (d) 129. The contour interval is 1 K.
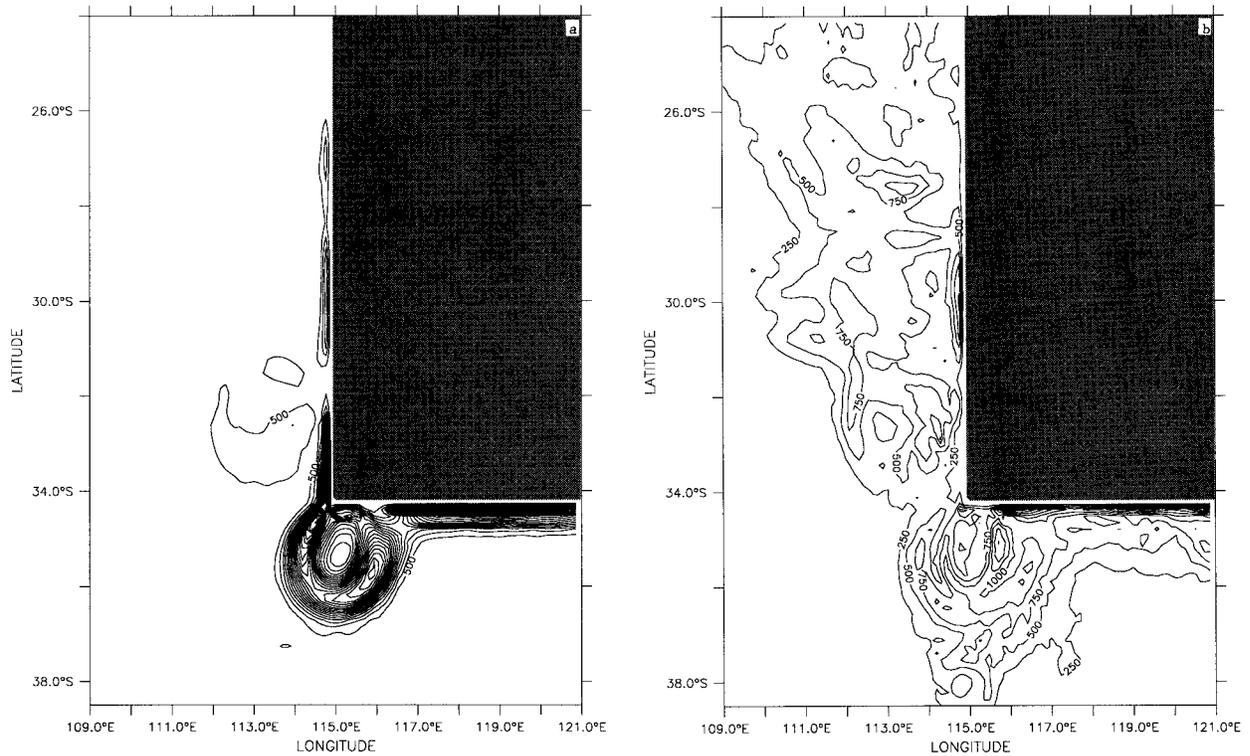
FIG. 9. Same as Fig. 5 except for experiment 3.

nisms dominant. This is also the case for subsequent eddy development.

Horizontal maps of the upper-layer MKE and EKE, averaged over the time period when the Leeuwin Current is strongest (~180 days), are shown in Figs. 11a and 11b. High values of MKE (Fig. 11a) are found offshore of coastal promontories, while lower values of MKE are found in the vicinity of coastal indentations. High values of EKE (Fig. 11b) are found all along the coastal and offshore regions of Western and Southern Australia. As in the previous experiments, the highest values of MKE and EKE are found in the coastal regions off Southern Australia.

e. Comparison with observations

Since experiments 2 and 4 incorporated realistic coastline geometry, it is useful to qualitatively compare the results of the model simulations with observational data. Since these studies are not model hindcasts but are idealized process-oriented studies, we cannot make direct comparisons with data; however, we can investigate whether the phenomenonological model behavior is qualitatively similar to observational data in the LCS. Note also that, although longer experimental runs of ~1000 days show that the system continues to generate currents and eddies in the LCS, here, since we are concentrating on the generation of currents and eddies in
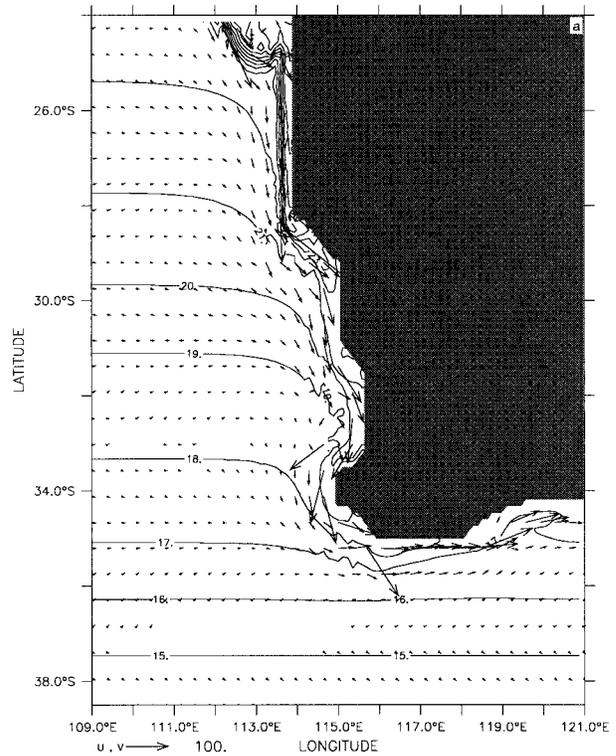
FIG. 10. Experiment 4 surface temperature and velocity vectors on day (a) 9, (b) 24, (c) 36, (d) 90, and (e) 120. The contour interval is 1 K.
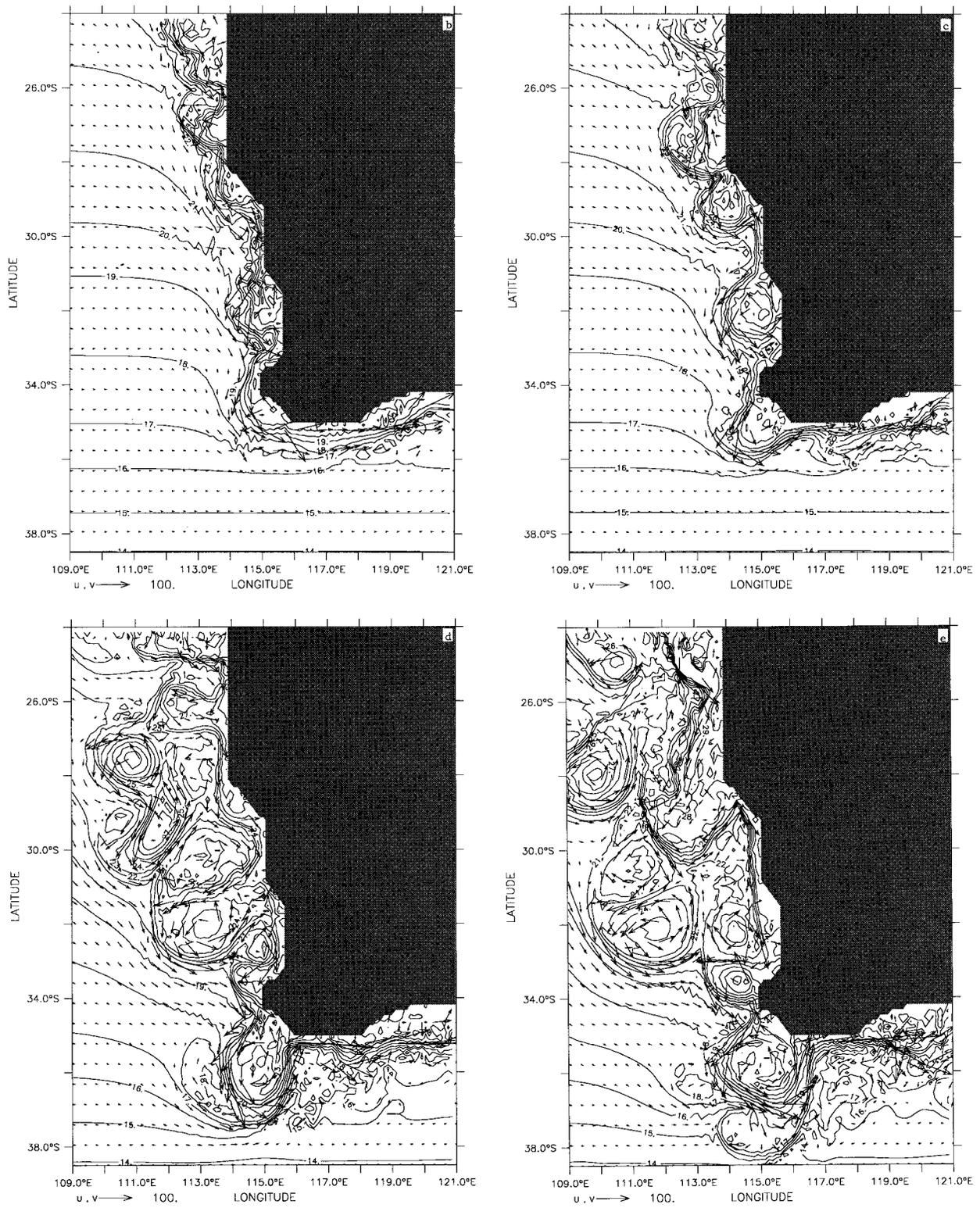
Fig. 10. (*Continued*)
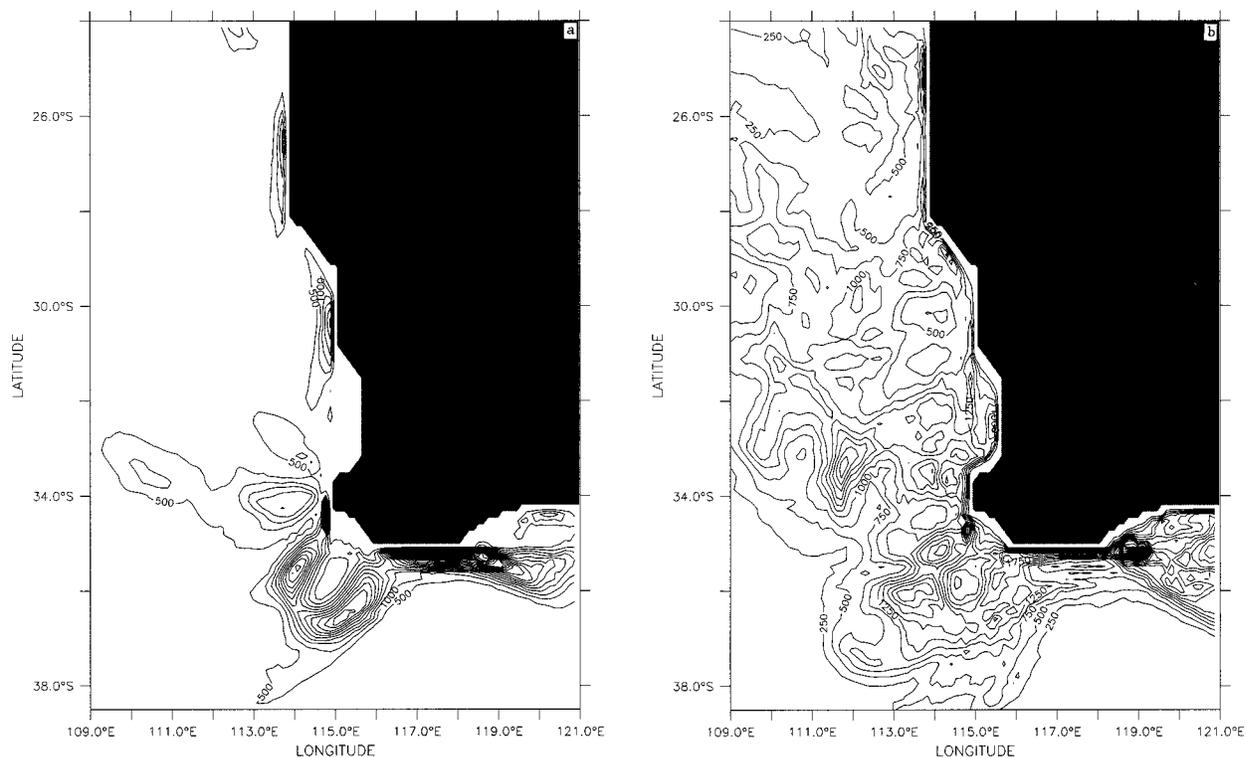
FIG. 11. Same as Fig. 5 except for experiment 4.
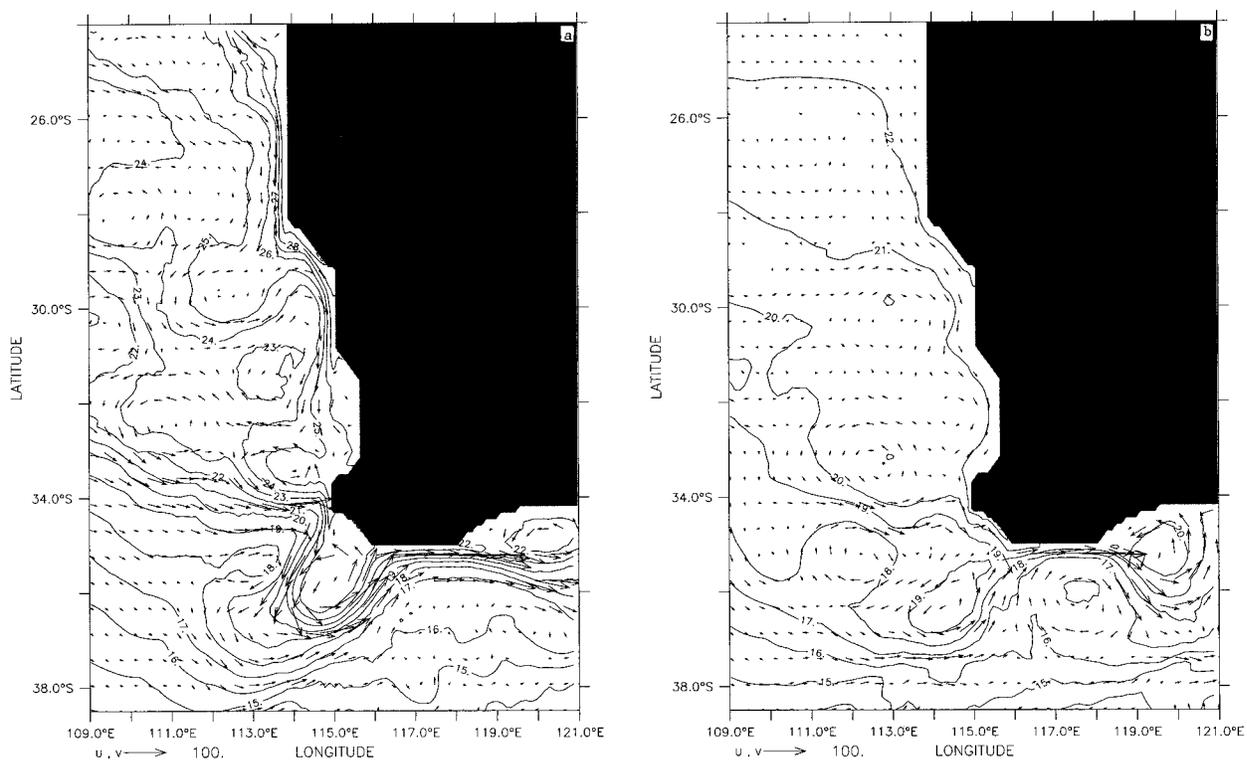
FIG. 12. Time-averaged surface temperature and velocity vectors from April to September (days 90–270) for (a) experiment 4 and (b) experiment 2. The contour interval is 1 K.
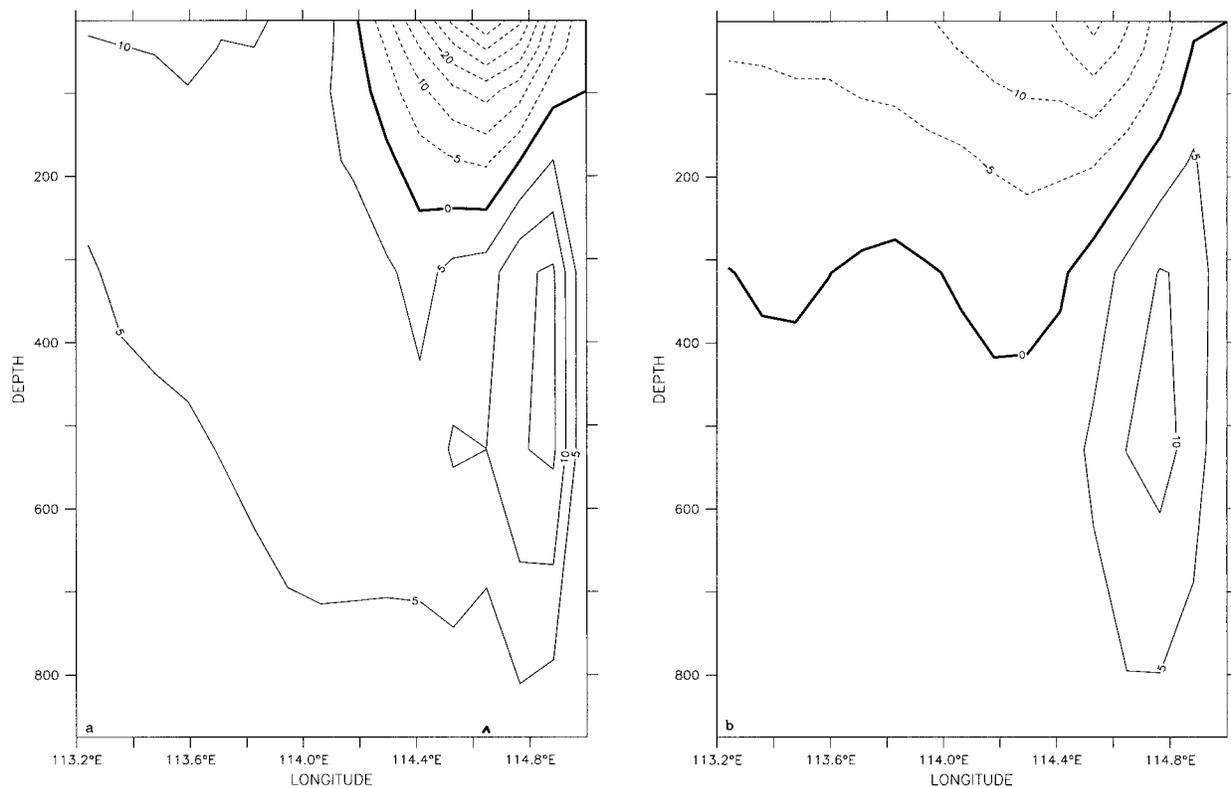
FIG. 13. Time-averaged cross-shore sections of the velocity field at 29.5°S from April to September (days 90–270) for (a) experiment 4 and (b) experiment 2. The contour interval is 5 K.

the LCS, we use results obtained during the first model year to compare with available observations.

Both instantaneous (Figs. 6 and 10) and time-averaged (Figs. 12–14) model results will be used in the comparison. The time-averaged plots have been taken over the time period that the Leeuwin Current is strongest (~April to September, corresponding to model days 90 to 270). General features of the Leeuwin Current are apparent from satellite images as well as measured current meter and hydrographic data. The discussion in the ensuing paragraphs details the general features and then discusses the specific magnitudes and characteristics along the Western and Southern Australian coast. Overall, the results of the experiment 4 complex flow regime highlights the major characteristics of the Leeuwin Current with relatively close similarities to field observations.

1) COMPARISON OF OCEAN CURRENTS

In experiments 2 and 4 the numerical model, through the use of climatological data, developed an ocean current that contained many features (e.g., Figs. 6, 10, and 12) observed in the LCS during the austral winter. The existence of an onshore geostropic flow, which starts as a broad fan-shaped form off northwestern Australia and then forms a narrow poleward current advecting warm tropical waters southward to Cape Leeuwin then eastward into the Great Australian Bight has been observed in numerous satellite images. These images reveal a system of meanders, eddies, alongshelf jets, and offshoots on a range of length scales (e.g., Pearce and Cresswell 1985; Church et al. 1986; Legeckis and Cresswell 1981; Griffiths and Pearce 1985; Cresswell and Peterson 1993). The observation that the Leeuwin Current is not a steady flow has been made by Legeckis and Cresswell (1981) and Pearce and Griffiths (1990). They both observed current surges, "jets," and large spatial variations due to intensification of instabilities. The experimental results document several current surges as well as large spatial variations in the current from Rossby wave propagation.

(i) The current off of Western Australia. The major characteristics of the modeled Leeuwin Current off Western Australia are consistent with field observations. For example, the sustained magnitudes of the model poleward (~5–40 cm s^{-1}) and equatorward (~5–15 cm s^{-1}) current (Fig. 13) compare favorably with LUCIE current meter data obtainied at Dongara (29.5°S) during the austral winter, which measured 38.5 cm s^{-1} for the poleward current, and 5.9 m s^{-1} for the undercurrent (e.g., Church et al. 1989; Boland et al. 1988; Smith et al. 1991). The model temperature cross section at 29.5°S
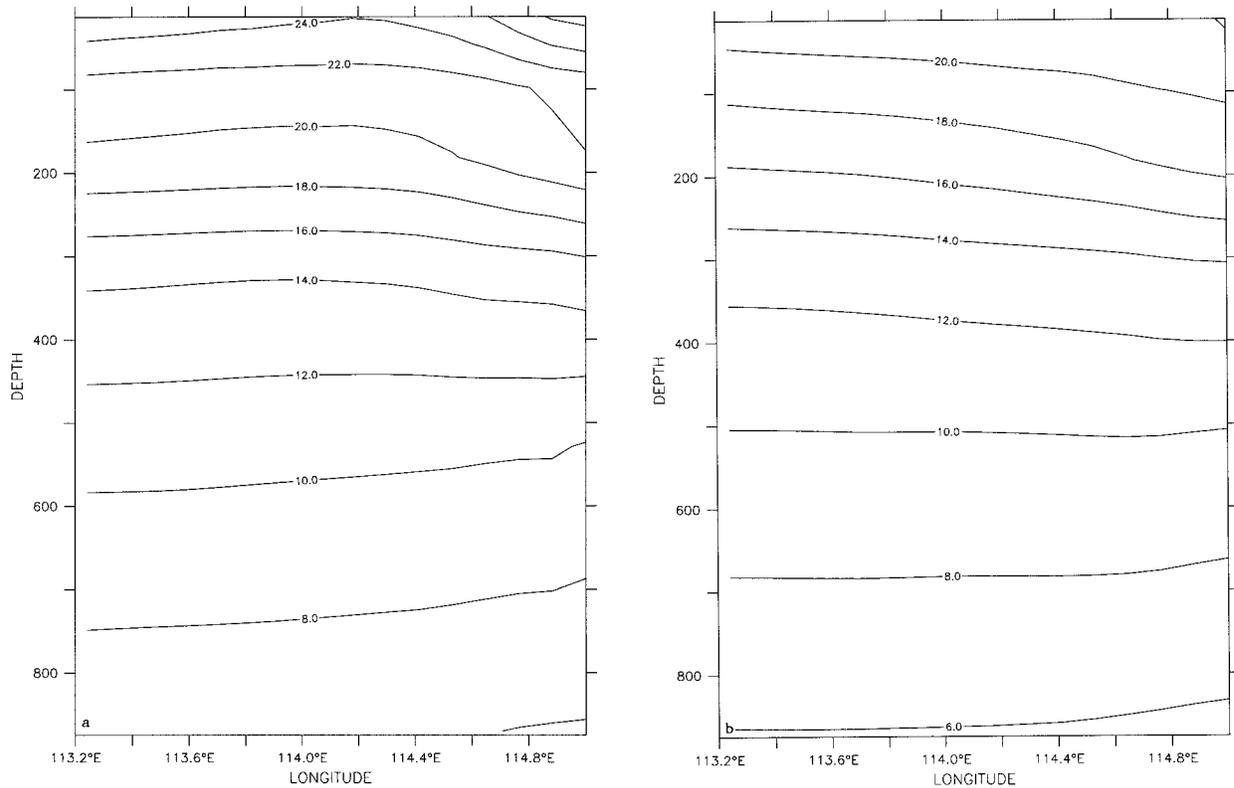
FIG. 14. Time-averaged cross-shore sections of the temperature field at 29.5°S from April to September (days 90–270) for (a) experiment 4 and (b) experiment 2. The contour interval is 2 K.

(Fig. 14), which shows downward (upward) sloping isotherms above (below) 400-m depth, are also consistent with CTD sections off of Dongara (e.g., Church et al. 1989).

With the inclusion of the NWS waters in experiment 4, the simulated poleward velocity increase to ~1.0 to 1.8 m s⁻¹ at Cape Leeuwin (e.g., Fig. 10) is consistent with surface current measurements greater than 1 m s⁻¹ measured by the RV *Franklin* at Cape Leeuwin (Cresswell and Peterson 1993). From the CTD measurements of Cresswell and Peterson (1993) it is observed that the NWS water increases coastline temperatures ~2–3 K by advecting warmer "tropical" waters. This observation is consistent with the 2–3 K difference noted by comparing the simulated temperature fields from experiment 2 (Fig. 12b), which had no NWS water, with the temperatures from experiment 4 (Fig. 12a), which had the addition of NWS water.

Experiment 4 also revealed how the irregular coastline limited the extent of the advection of NWS water along the Australian coast. This is consistent with satellite images (e.g., Church et al 1989), which show that the bulk of NWS water is arrested north of Dongara. These observations support the model results for current characteristics off of Western Australia.

(ii) The current off of Southern Australia. Griffiths and Pearce (1985) used high-resolution infrared images from *NOAA-7* to reveal that the poleward flow off the west coast of Australia moves against the coastline as it approaches Cape Leeuwin and continues to hug the coast as it flows eastward. They also observed that the largest current velocities (~1.8 m s⁻¹) along the southern coast of Australia occurs near Cape Leeuwin where the dynamics is influenced by the 90° corner. Godfrey et al. (1986) noted the strongly nonlinear dynamics in the neighborhood of Cape Leeuwin. All of the experiments showed this dynamic shift, along with maximum currents and an undercurrent that occurred in the vicinity of Cape Leeuwin. The magnitude of the model eastward surface current was ~1–1.7 m s⁻¹ in experiment 4, which is closest in agreement with current meter measurements from Cresswell and Peterson (1993) that showed eastward surface velocities of 1–1.6 m s⁻¹.

The inclusion of the NWS waters in the model act to drive warmer waters into the Great Australian Bight and to intensify the current velocity and temperature fronts (e.g., Figs. 10 and 12a). This is consistent with observations. For example, Rochford (1986) observed that the Leeuwin Current carries the warmest water mass into the Great Australia Bight as far as 130°E, while Pearce and Cresswell (1985) observed that in the austral winter a surface temperature gradient up to 5°C may be encountered in the Leeuwin to Esperance region.

2) COMPARISON OF EDDIES

Consistent with the buoy observations of Cresswell and Golding (1979, 1980) and satellite observations of Griffiths and Pearce (1985), eddy generation occurs on the offshore side of the core of the Leeuwin Current. In experiments 2 and 4, the onset of instabilities occurs at preferred locations (e.g., Figs. 6 and 10). These locations were where the coastline significantly changed, that is, near Shark Bay, between Dongara and Fremantle, Cape Leeuwin, and off the coast of Albany. Figure 3 of Pearce and Griffiths (1991) and Fig. 11.21(a) of Tomzcak and Godfrey (1994) show satellite images that agree with the west coast preferred locations for the formation of meanders and eddy positions, while Fig. 11.21(b) of Tomzcak and Godfrey (1994) shows a satellite image that agrees with the south coast locations for the formation of meanders and eddies. The images also show a preference of warm, anticyclonic eddies to exist at the coast. In the LCS, in agreement with the model simulations, observations show that the eddies have timescales of months, can be anticyclonic or cyclonic, and can exist in pairs or as a separate entity (Hamon 1965, 1972; Condie and Ivey 1988; Pearce and Griffiths 1991).

The eddy wavelengths of O(100 km) simulated in the model are close to the wavelengths associated with a low-mode Rossby radius of deformation (of ~30 km). These lengths are also consistent with observations (e.g., Hamon and Cresswell 1972; Golding and Symond 1977; Griffiths and Pearce 1985), and laboratory studies (e.g., Condie and Ivey 1988) of eddies in the Leeuwin Current.

4. Summary

The use of process-oriented modeling studies of the LCS off Western and Southern Australia has been instrumental in providing insight into the development of unique current characteristics and mesoscale features. In all experiments, a poleward and eastward surface current, an equatorward undercurrent, offshoots, meanders, and eddies were generated. Maximum surface velocities occurred at Cape Leeuwin and off Southern Australia, while maximum undercurrent velocities occurred off Western Australia. The offshoots, anticyclonic meanders, and anticyclonic eddies were generated at preferred locations: off Cape Leeuwin and the Western Australian coast in the ideal coastline experiments (cases 1 and 3) and off Cape Leeuwin and in the vicinity of coastal promontories in the realistic coastline experiments (cases 2 and 4).

The results of experiment 1 (ideal coastline) revealed how current dynamics around Cape Leeuwin increase instability by inducing anticyclonic vorticity into the system. This anticyclonic vorticity is likely a result of the current shifting from poleward to eastward via the Coriolis and geostrophic forces acting on the current.

The 90-degree corner (Cape Leeuwin) was the preferred location for the development of initial mesoscale features; subsequent mesoscale features developed upstream of Cape Leeuwin. Results for the instability analysis showed that mixed instability mechanisms were present in the coastal region off Western Australia, while barotropic instability dominated in the coastal regions off Cape Leeuwin and Southern Australia. Horizontal maps of the upper-layer MKE and EKE kinetic energy showed that high values of MKE and EKE were found off Southern Australia, while high values of EKE were also found south of 30°S. Overall, the MKE was higher than the EKE. This is consistent with the model simulations, which showed that the eddies were generated from instabilities of the mean currents via barotropic and/or baroclinic instability processes.

In experiment 2, the irregular (realistic) coastline limited the extent of advection of warmer waters along the entire coast. Initial eddy development occurred much earlier and developed in preferred locations: at Shark Bay, between Dongara and Fremantle, and at Cape Leeuwin (in the vicinity of coastal promontories along Western Australia and Cape Leeuwin). The results of the instability analysis showed that mixed instability was responsible for the generation of the eddies, with barotropic instability dominant over baroclinic instability. Maps of MKE and EKE showed that the highest values were found in the coastal regions off Southern Australia.

The added contribution from the North West Shelf water in cases 3 and 4 augmented the onshore geostrophic flow to produce a model Leeuwin Current and undercurrent, which were more vigorous and unstable than in the previous cases. In experiment 3, the NWS water added strong horizontal shear to the coastal equatorial region of the domain and vertical shear to the inshore current. The NWS water addition advected warmer water along the entire coastal boundary and resulted in the advection of warmer waters offshore by the anticyclonic eddies. While mixed instability mechanisms with the barotropic mechanism dominant were responsible for most regions of eddy development as in the previous cases, baroclinic instability dominated over barotropic instability mechanims off Western Australia. This could be caused by the interaction of northern eddy pairs propagating westward and the onshore eastward geostrophic flow with the result that vertical shear regions were generated. Maps of MKE and EKE showed that the highest values of MKE and EKE were found off Cape Leeuwin and Southern Australia. In contrast to the previous cases, high values of EKE were found all along the Western Australian coastal and offshore regions. This is likely due to the NWS addition, which added significant instability to the source region and throughout the coastal region of Western Australia.

In experiment 4, the addition of both the NWS water and the irregular coastline resulted in the establishment of a stronger surface current and undercurrent than in

the previous cases; however, the irregular coastline limited the extent of the advection of the NWS warmer water along the Australian coast. Maps of the upper-layer MKE and EKE showed that high values of MKE were found offshore of coastal promontories, while lower values of MKE were found in the vicinity of coastal indentations. High values of EKE were found all along the coastal and offshore regions of Western and Southern Australia. The highest values of MKE and EKE were found in the coastal regions off Southern Australia.

In all cases, warm, anticyclonic eddies developed at the coast. Cold, cyclonic eddies formed from the limbs of the established warm, anticyclonic eddies with the result that two counterrotating cells were developed. Once the eddy pairs began their westward propagation, the Leeuwin Current intensified as nonlinear effects resulted in a jet between the eddies and the coast. These effects translated downstream to augment the current velocities at the coast, which, due to a mixed instability mechanism, resulted in the development of new anticyclonic eddies at the coast.

The results from experiment 4, which had the most realistic features, highlighted the major characteristics of the Leeuwin Current and agreed well with available observations off Western and Southern Australia. These results show that the model successfully captures the qualitative nature of the nonlinear, eddying response of the Leeuwin Current.

REFERENCES

Arakawa, A., and V. R. Lamb, 1977: Computational design of the basic dynamical processes of the UCLA general circulation model. *Methods in Computational Physics,* J. Chang, Ed., Academic Press, 173–265.

Batteen, M. L., 1997: Wind-forced modeling studies of currents, meanders, and eddies in the California Current System. *J. Geophys. Res.,* **102,** 985–1010.

——, and Y.-J. Han, 1981: On the computational noise of finite-difference schemes used in ocean models. *Tellus,* **33,** 387–396.

——, M. J. Rutherford, 1990: Modeling studies of eddies in the Leeuwin Current: The role of thermal forcing. *J. Phys. Oceanogr.,* **20,** 1484–1520.

——, R. L. Haney, T. A. Tielking, and P. G. Renaud, 1989: A numerical study of wind forcing of eddies and jets in the California Current System. *J. Mar. Res.,* **47,** 493–523.

——, ——, and E. J. Bayler, 1992: A numerical study of wind- and thermal-forcing effects on the ocean circulation off Western Australia. *J. Phys. Oceanogr.,* **22,** 1406–1433.

Boland, F. M., J. A. Church, A. M. G. Forbes, J. S. Godfrey, A. Huyer, R. L. Smith, and N. J. White, 1988: Current-meter data from the Leeuwin Current Interdisciplinary Experiment. CSIRO Marine Laboratories Rep. 198, 31 pp.

Camerlengo, A. L., and J. J. O'Brien, 1980: Open boundary conditions in rotating fluids. *J. Comput. Phys.,* **35,** 12–35.

Church, J. A., G. R. Cresswell, and J. S. Godfrey, 1989: The Leeuwin Current. *Poleward Flows along Eastern Ocean Boundaries,* S. Neshyba, C. N. K. Mooers, R. I. Smith, and R. T. Barber, Eds., Springer-Verlag, 230–252.

Condie, S. A., and G. N. Ivey, 1988: Convectively driven coastal current in a rotating basin. *J. Mar. Res.,* **46,** 476–494.

Cresswell, G. R., and T. J. Golding, 1979: Satellite-tracked buoy data report III. Indian Ocean 1977, Tasman Sea July–December 1977. CSIRO Australia Division of Fisheries and Oceanography Rep. 101.

——, and ——, 1980: Observations of a south-flowing current in the southeastern Indian Ocean. *Deep-Sea Res.,* **27A,** 449–466.

——, and J. L. Peterson, 1993: The Leeuwin Current south of Western Australia. *Aust. J. Mar. Freshwater Res.,* **44,** 285–303.

Gentilli, J., 1972: Thermal anomalies in the eastern Indian Ocean. *Nature (London) Phys. Sci.,* **238,** 93–95.

Godfrey, J. S., and K. R. Ridgway, 1985: The large-scale environment of the poleward-flowing Leeuwin Current, Western Australia: Longshore steric height gradients, wind stresses, and geostrophic flow. *J. Phys. Oceanogr.,* **15,** 481–495.

——, D. J. Vaudrey, and S. D. Hahn, 1986: Observations of the shelf-edge current south of Australia winter 1982. *J. Phys. Oceangr.,* **16,** 668–679.

Golding, T. J., and G. Symonds, 1978: Some surface circulation features off Western Australia during 1973–1976. *Aust. J. Mar. Freshwater Res.,* **29,** 187–191.

Griffiths, R. W., and A. F. Pearce, 1985: Instability and eddy pairs on Leeuwin Current south of Australia. *Deep-Sea Res.,* **32,** 1511–1534.

Hamon, B. V., 1965: Geostrophic currents in the south-eastern Indian Ocean. *Austr. J. Mar. Freshwater Res.,* **16,** 255–271.

——, 1972: Geopotential topographies and current off West Australia, 1965–69. CSIRO Division of Fisheries and Oceanography, Tech. Paper No. 32, 11 pp. [Available from CSIRO Marine Laboratories, GPO Box 1538, Hobart, Tasmania 7001, Australia.]

Hamon, B. V., and G. R. Cresswell, 1972: Structure functions and intensities of ocean circulation off east and west Australia. *Aust. J. Mar. Freshwater Res.,* **23,** 99–103.

Hirst, A. C., and J. S. Godfrey, 1993: The role of Indonesian Throughflow in a global ocean GCM. *J. Phys. Oceanogr.,* **23,** 1057–1086.

Holland, W. R., 1978: The role of mesoscale eddies in the general circulation of the ocean-numerical experiments using a wind-driven quasigeostrophic model. *J. Phys. Oceanogr.,* **8,** 363–392.

——, and M. L. Batteen, 1986: The parameterization of subgrid scale heat diffusion in eddy-resolved ocean circulation models. *J. Phys. Oceanogr.,* **16,** 200–206.

——, D. E. Harrison, and A. J. Semtner Jr. 1983: Eddy-resolving numerical models of large-scale ocean circulation. *Eddies in Marine Science,* A. R. Robinson, Ed., Springer-Verlag, 379–403.

Legeckis, R., and G. R. Cresswell, 1981: Satellite observations of sea surface temperature fronts off the coast of Western and South Australia. *Deep-Sea Res.,* **28A,** 297–306.

Levitus, S., 1982: *Climatological Atlas of the World Ocean.* NOAA Professional Paper No. 13, U.S. Govt. Printing Office 173 pp.

——, and T. P. Boyer, 1994: *World Ocean Atlas.* Vol. 4:*Temperature,* NOAA Atlas NESDIS 4, U.S. Department of Commerce, National Oceanic and Atmospheric Administration, 117 pp.

McCreary, J. P., Jr., S. R. Shetye, and P. K. Kundu, 1986: Thermohaline forcing of eastern boundary currents: With application to the circulation off the west coast Australia. *J. Mar. Res.,* **44,** 71–92.

Pearce, A. F., and G. R. Cresswell, 1985: Ocean circulation off Western Australia and the Leeuwin Current. CSIRO Information Service Sheet No. 16-3, 4 pp. [Available from CSIRO Marine Laboratories, GPO Box 1538, Hobart, Tasmania 7001, Australia.]

——, and R. W. Griffiths, 1991: The mesoscale structure of the Leeuwin Current: A comparison of laboratory models and satellite imagery. *J. Geophys. Res.,* **96,** 16 739–16 757.

Rochford, D. J., 1986: Seasonal changes in the distribution of Leeuwin Current waters off southern Australia. *Austr. J. Mar. Freshwater Res.,* **37,** 1–10.

Semtner, A. J., and Y. Mintz, 1977: Numerical simulation of the Gulf Stream and midocean eddies. *J. Phys. Oceanogr.,* **7,** 208–230.

Smith, R. L., A. Huyer, J. S. Godfrey, and J. A. Church, 1991: The Leeuwin Current off Western Australia, 1986–1987. *J. Phys. Oceanogr.,* **21,** 323–345.

Thompson, R. O. R. Y., 1987: Continental-shelf-scale model of the Leeuwin Current. *J. Mar. Res.,* **45,** 813–827.

Tomczak, M., and J. S. Godfrey, 1994: Eastern boundary currents. *Regional Oceanography: An Introduction,* Pergamon Press, 217–220.

Weatherly, G. L., 1972: A study of the bottom boundary layer of the Florida Current. *J. Phys. Oceanogr.,* **2,** 54–72.